Mechanism and Machine Theory 87 (2015) 18–44

Contents lists available at ScienceDirect

Mechanism and Machine Theory

journal homepage: www.elsevier.com/locate/mechmt

Research on a tracked omnidirectional and cross-country vehicle

Yunan Zhang, Tao Huang *

Department of Control Engineering, Academy of Armored Forces Engineering, No. 21, Du Jiakan, Fengtai District, Beijing 100072, China

ARTICLE INFO

Article history:
Received 3 August 2014
Received in revised form 23 December 2014
Accepted 30 December 2014
Available online 10 January 2015

Keywords:
Track running mechanism
Omnidirectional vehicle
Cross-country

ABSTRACT

Conventional tracked vehicles have superior cross-country capability compared to common wheeled vehicles, but poor maneuverability, especially poor steering performance. However, the existing omnidirectional vehicles have poor cross-country capability despite much higher maneuverability than common vehicles. This paper presents an innovational track running mechanism, a vehicle construction and its unique kinematical and dynamical theories, with an independent electric drive system used to construct a tracked omnidirectional and cross-country vehicle — a tracked-omni-vehicle. The vehicle demonstrates omnidirectional motion on uneven terrains, superior steering efficiency, equal longitudinal motion efficiency, and comparable cross-country performance in comparison to conventional tracked vehicles. The success of the tracked-omni-vehicle has made a breakthrough in the running mode of conventional tracked vehicles and the limitations of omnidirectional vehicles in engineering applications.

1. Introduction

Omnidirectional vehicles are a type of 3 degree of freedom (DOF) vehicles on the ground. They can achieve longitudinal motion, lateral motion, center-point steering motion, and any composite motion of above three, so they are suitable for highly maneuverable, narrow or accurate positioning occasions. Omnidirectional vehicles are characterized by their special running mechanisms. At present, most researchers are mainly focusing research on the wheeled omnidirectional running mechanisms, such as Mecanum wheel, alternate wheel, and ball wheel [1]. Especially, Mecanum wheeled omnidirectional vehicles have been widely used in military [2], storage and transportation [3], social services [4], and other fields, for example the omnidirectional forklift as shown in Fig. 1. However, the wheeled omnidirectional vehicles still have significant limitations in engineering applications despite much higher maneuverability than common wheeled vehicles, because there are some common problems with them. Taking the omnidirectional forklift for example, the problems are as follows:

- Large vibrations. The Mecanum wheel is almost rigid and its ground contact roller is discontinuously changing, so the forklift has large vibrations, even on the flat ground.
- Limited loading capacity. The ground contact area of the Mecanum wheel is extremely small, so the ground pressure is extremely large in the case of heavy loads.
- High road conditions. The omnidirectional forklift is not suitable for running on uneven terrains, and can only work on flat and hard surfaces.

Inversely, conventional tracked vehicles, such as bulldozers, excavators, tanks, and tractors, have stable movements, large loading capacity, and superior cross-country capability to common wheeled vehicles and they are capable of crossing obstacles, trenches or breaks, and are much less likely to get stuck in soft ground. However, they are inferior to wheeled vehicles in their maneuverability,

* Corresponding author. Tel.: +86 18611973725, +86 10 66718706.
E-mail addresses: zhang_yunan@sina.com (Y. Zhang), wdmd_huang@126.com (T. Huang).

http://dx.doi.org/10.1016/j.mechmachtheory.2014.12.016
0094-114X/

Fig. 1. The omnidirectional forklift.

and are especially difficult to steer because of great lateral resistances [5]. In order to promote the steering performance of tracked vehicles, many researchers have carried out a lot of studies on steering gears, control strategies, and so on [5–7], but the results remain unsatisfactory. Furthermore, it is incredible that conventional tracked vehicles can run with omnidirectional motion. Although some researchers have developed several kinds of impressive tracked running mechanisms for omnidirectional motion as shown in Fig. 2, including the omnidirectional spherical tire track [8], the Vuton crawler [9], the crawler–roller running mechanism [10,11], and the omni-crawler [12,13], they have some different problems as follows:

1. Omnidirectional spherical tire track. It consists of several balls and a pair of parallel rods. Motion in the longitudinal direction is achieved by moving the balls along the length of rods; sliding is prohibited and thus the balls rotate about the axes parallel to the lateral direction. Motion in the lateral direction is achieved by rotating the rods about their axes, which in turn rotates the balls about the axes parallel to the longitudinal direction. A vehicle equipped with such two tracks can achieve omnidirectional motion, but has difficulty crossing obstacles in either a longitudinal direction or a lateral direction. Additionally, each ball requires a different angular velocity vector in steering motion, but all balls in the same track are constrained to move with the same angular velocity vector. Consequently, it has large steering lateral resistance which is the same as that of an equivalent conventional tracked vehicle.
2. Vuton crawler. The free rollers of the Vuton crawler are supported by square frame members with rotational motion independence, and the square frame members are connected to the chains at diagonal points separated by a horizon distance. The pair of chains is also offset with the same distance, and the chains are driven simultaneously. A vehicle equipped with such four crawlers can achieve omnidirectional motion, but it has a square layout, which is inapplicable to conventional tracked vehicles. Additionally, such a vehicle has difficulty crossing obstacles, and its gradeability is also inferior to that of a conventional tracked vehicle. Fortunately, it almost causes no wear on the ground in steering motion, because of extremely little lateral resistance [14].
3. Crawler–roller running mechanism. Its free rollers are mounted on the outside with two of them constituting one unit. It has the same running principle as the Vuton crawler, so a vehicle equipped with such four mechanisms also has a square layout. Such a vehicle can steadily run on uneven terrains and cross some small obstacles, but its crossing obstacle is limited to the diameter of the roller, which is much smaller than that of the crawler. Although the smaller rollers that are mounted on the rollers can play a role in crossing some higher obstacles, its ability to cross obstacles is still inferior to that of an equivalent conventional tracked vehicle.
4. Omni-crawler. It is characterized by a circular cross-section. The crawler module has an active rotational axis, which allows it to achieve lateral motion. When the axis of the driving sprocket is perpendicular to the ground, there is a singularity that does not allow for the generation of any longitudinal traction. If the lateral motion is active in an invariant direction, the direction of longitudinal motion will be changed after crossing the singularity. Its control for omnidirectional motion is unrealistic, because the singularities should be sensed and the rotational directions of the sprockets should also be changed frequently. Therefore, the vehicle has difficulty achieving a diagonal motion and can only perform the longitudinal and lateral motion independently. Additionally, it also has large steering lateral resistance which is the same as that of an equivalent conventional tracked vehicle, because all ground contact points on one crawler are constrained to move with the same velocity vector.

In brief, the existing tracked omnidirectional running mechanisms are impossible to apply to conventional tracked vehicles, because the vehicles equipped with such running mechanisms cannot retain the cross-country capability of conventional tracked vehicles, and have inapplicable vehicle construction or unrealistic motion control.

In order to resolve the problems associated with the omnidirectional vehicles and improve the maneuverability of conventional tracked vehicles, a novel tracked running mechanism has been proposed in this paper, with which a tracked vehicle can not only achieve omnidirectional motion to improve the maneuverability of conventional tracked vehicles but also retain the cross-country

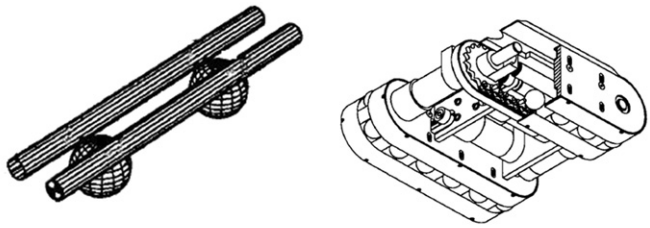

(a) Omnidirectional spherical tire track

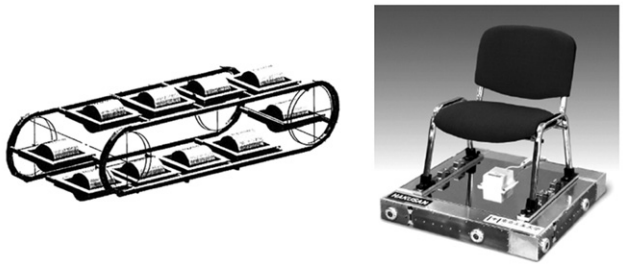

(b) VUTON crawler

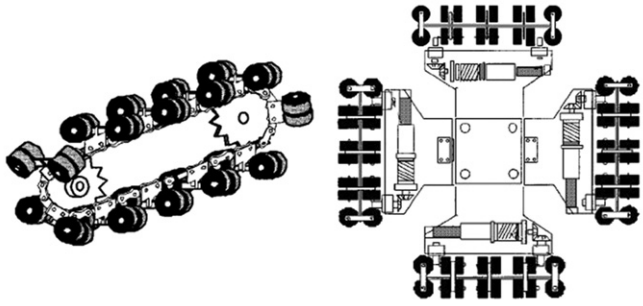

(c) Crawler-roller running mechanism

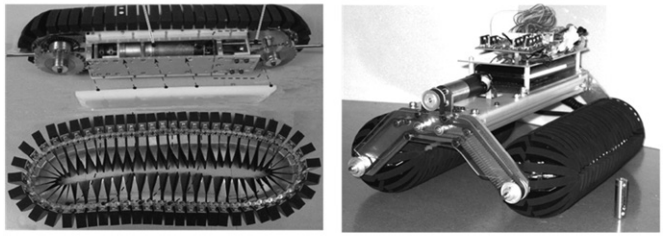

(d) Omni-crawler

Fig. 2. Illustrations of existing tracked omnidirectional running mechanisms and their vehicles.

capability of conventional tracked vehicles. Additionally, this paper also presents an aggregation of innovations in kinematical and dynamical theories to create a tracked omnidirectional and cross-country vehicle — a tracked-omni-vehicle.

2. The tracked-omni-vehicle

2.1. Structure principle of the omni-track

Based on the analysis of existing omnidirectional running mechanisms, a new tracked running mechanism has been invented, namely, omni-track. It has a structure similar to a conventional mechanism, including a track, drive sprockets, road wheels, and return wheels as shown in Fig. 3. Along the track, each track plate is connected to the rest with hinge-type pins, but it is crucially different in that small cylindrical rollers take the place of the track grousers present in conventional tracks. The rollers are mounted in an offset angle α $(0 < \alpha < \pi/2)$ and can rotate freely, so the omni-track has 2 DOFs on the ground, one of which is in the winding (longitudinal) direction, while the other is perpendicular to the axes of the ground contact rollers. Additionally, with consideration to the ground contact area, there is no limit to the number of rollers' columns, such as one, two, or more.

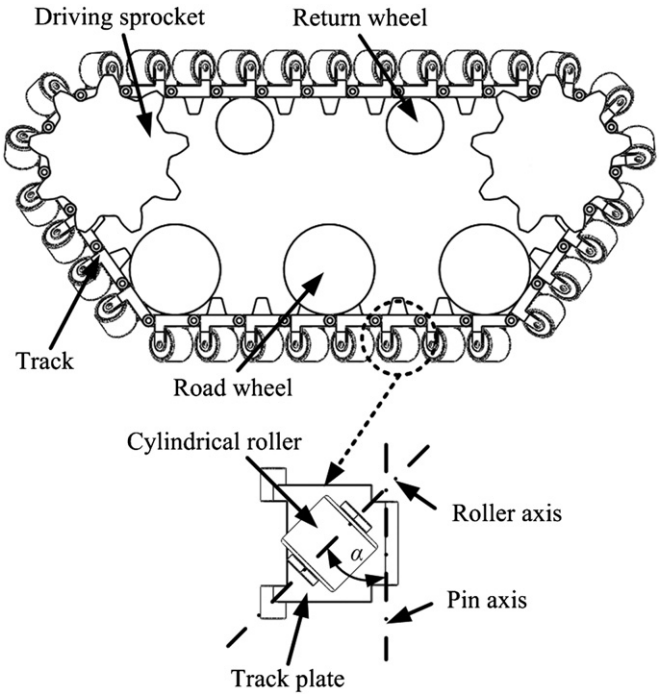

Fig. 3. The structure principle of the omni-track.

2.2. Kinematics analysis of the tracked-omni-vehicle

2.2.1. Kinematics analysis of the omni-track

The motion of a track is a kind of composite motion, which consists of following and relative motions. Following motion refers to the motion of the track following the body of a vehicle and relative to the ground, and relative motion refers to the motion of the track relative to the body. Define following velocity vector as v_q, relative velocity vector as v_l, and absolute velocity vector as v_f, hence,

$$v_f = v_q + v_l. \tag{1}$$

The omni-track has 2 DOFs on the ground, so its relative velocity vector is synthesized from velocity vectors in two directions. First, analyze the velocity vectors of any ground contact point o'' on a plane as shown in Fig. 4.

In the figure, $x'o'y'$ is the coordinate of center point o' of the drive sprocket, $x''o''y''$ is the coordinate of the point o'', and $o'x'//o''x''$. Define ω as the angular velocity vector of the driving sprocket, r as the radius of the drive sprocket, v_m as the winding velocity vector of the track, $v_{mo''}$ as the relative velocity vector of point o'' in the y'' direction, and v_r as the relative velocity vector of point o'' in the direction perpendicular to the axis of the roller.

Assume that the track is a soft belt without elasticity, the ground is flat, and the ground contact segment of the track is rigid, then:

$$v_m = \omega r = v_{mo''}. \tag{2}$$

Hence, the relative velocity vector of point o'' is:

$$v_l = v_{mo''} + v_r. \tag{3}$$

Assume that there is no slippage on the ground contact segment, then:

$$v_q = -v_l. \tag{4}$$

Define the parameters as follows:

v'_{qy} Magnitude of the component vector of v_q in the y'' direction;
v'_{qx} Magnitude of the component vector of v_q in the x'' direction.

Combining Eqs. (2), (3), and (4):

$$\begin{pmatrix} v''_{qy} \\ v''_{qx} \end{pmatrix} = \begin{pmatrix} r - \cos\alpha \\ 0 \quad \sin\alpha \end{pmatrix} \begin{pmatrix} \omega \\ v_r \end{pmatrix} = R_1 \begin{pmatrix} \omega \\ v_r \end{pmatrix}. \tag{5}$$

2.2.2. Basic construction of the tracked-omni-vehicle

The Jacobian matrix of the inverse kinematical equation of a system indicates the relation between the velocities of the system and its joints. When the column rank of the Jacobian matrix is unfilled, there is a singular configuration with the system [15]. For an omnidirectional (3 DOFs) vehicle on the ground, there should not be any singular configuration. Hence, the essential condition of omnidirectional motion is that the column rank of the Jacobian matrix must be filled and is equal to three [16].

Assume that a vehicle is constructed with $n(n = 1, 2, 3, \cdots)$ omni-tracks and each omni-track is equipped with multi-columned rollers, the velocity relation between the number $i(i = 1, 2, 3 \cdots, n)$ track and the vehicle was analyzed as shown in Fig. 5.

In the figure, the dotted rectangle denotes the ground contact segment of the track, and oblique lines indicate the axes of the rollers. Because the length of a roller is much shorter than the length of the ground contact segment, to simplify the analysis, each roller is considered as a point. The point o''_i is the geometrical center point of the ground contact segment, the point B is any ground contact point, xoy is the vehicle coordinate, and $x''_i o''_i y''_i$ is the track coordinate. Define $(v_y \quad v_x \quad \omega_z)^{\mathrm{T}}$ as the velocity of the center point o of the vehicle in the xoy coordinate, $\left(v''_y \quad v''_x\right)^{\mathrm{T}}$ as the following velocity of the point B in the xoy coordinate, $(l_{iy} \quad l_{ix} \quad \theta_i)^{\mathrm{T}}$ as the position of the $x''_i o''_i y''_i$ coordinate in reference to the xoy coordinate, $(l_{y''} \quad l_{x''})^{T}$ as the position of the point B in the $x''_i o''_i y''_i$ coordinate, l_i as the distribution distance from the point o'_i to the point o, β_i as the distribution angle, l_t as the length of the ground contact segment, and w_t as the width of the ground contact segment.

For the point B, there are:

$$\begin{pmatrix} v''_y \\ v''_x \end{pmatrix} = \begin{pmatrix} \cos\theta_i & \sin\theta_i \\ -\sin\theta_i & \cos\theta_i \end{pmatrix} \begin{pmatrix} v''_{qy} \\ v''_{qx} \end{pmatrix} = R_2 \begin{pmatrix} v''_{qy} \\ v''_{qx} \end{pmatrix} \tag{6}$$

$$\begin{pmatrix} v''_y \\ v''_x \end{pmatrix} = \begin{pmatrix} 1 & 0 & l_{ix} + l_{x''}\cos\theta_i - l_{y''}\cos\theta_i \\ 0 & 1 & -\left(l_{iy} + l_{x''}\sin\theta_i + l_{y''}\cos\theta_i\right) \end{pmatrix} \begin{pmatrix} v_y \\ v_x \\ \omega_z \end{pmatrix} = R_3 \begin{pmatrix} v_y \\ v_x \\ \omega_z \end{pmatrix}. \tag{7}$$

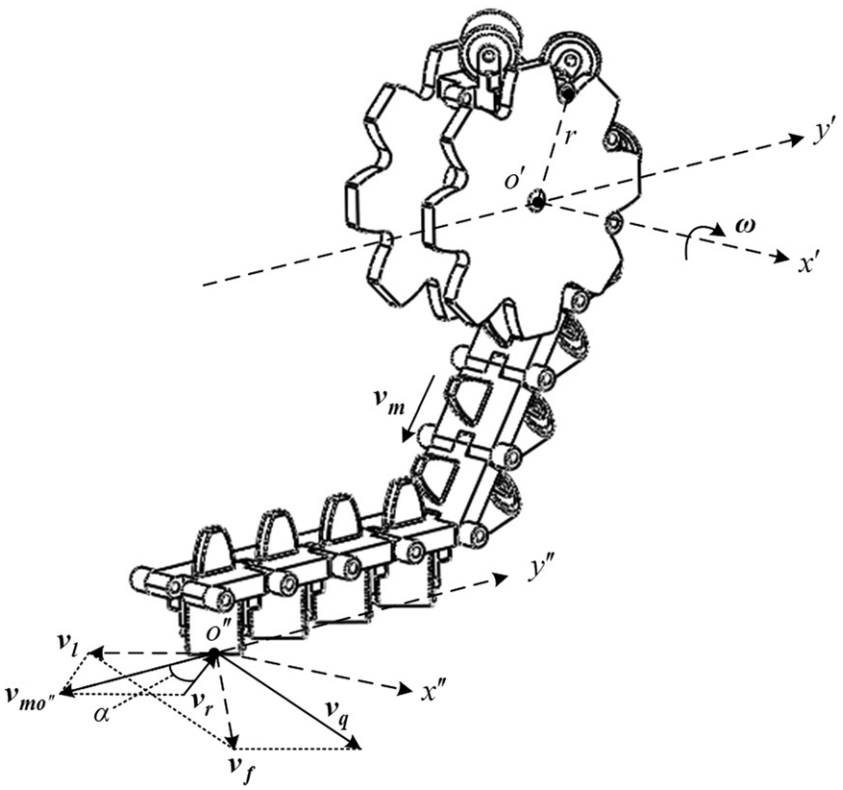

Fig. 4. Symbols for velocity analysis of any ground contact point.

For $\det(R_1 \neq 0)$, and $\det(R_2) \neq 0$, combining Eqs. (5), (6), and (7):

$$\begin{pmatrix} w \\ v_r \end{pmatrix} = \begin{pmatrix} \frac{\sin(\theta_i+\alpha_i)}{r\sin\alpha_i} & \frac{\cos(\theta_i+\alpha_i)}{r\sin\alpha_i} & \frac{\sin(\theta_i+\alpha_i)l_{ix}-\cos(\theta_i+\alpha_i)l_{iy}+l_{x''}\sin\alpha_i-l_{y''}\cos\alpha_i}{r\sin\alpha_i} \\ \frac{\sin\theta_i}{\sin\alpha_i} & \frac{\cos\theta_i}{\sin\alpha_i} & \frac{\sin\theta_i l_{ix}-\cos\theta_i l_{iy}-l_{y''}}{\sin\alpha_i} \end{pmatrix} \begin{pmatrix} v_y \\ v_x \\ \omega_z \end{pmatrix} \tag{8}$$

where $l_{x''}$ and $l_{y''}$ are variables.

And there is:

$$\begin{cases} l_{x''} \in \left[-\frac{w_t}{2}, \frac{w_t}{2}\right] \\ l_{y''} \in \left[-\frac{l_t}{2}, \frac{l_t}{2}\right] \end{cases}. \tag{9}$$

Define two continuous functions as follows:

$$\begin{cases} f_i\left(l_{x''}, l_{y''}\right) = \frac{\sin(\theta_i+\alpha_i)l_{ix}-\cos(\theta_i+\alpha_i)l_{iy}+l_{x''}\sin\alpha_i-l_{y''}\cos\alpha_i}{r\sin\alpha_i} \\ g_i\left(l_{x''}, l_{y''}\right) = \frac{\sin\theta_i l_{ix}-cos\theta_i l_{iy}-l_{y''}}{\sin\alpha_i} \end{cases}. \tag{10}$$

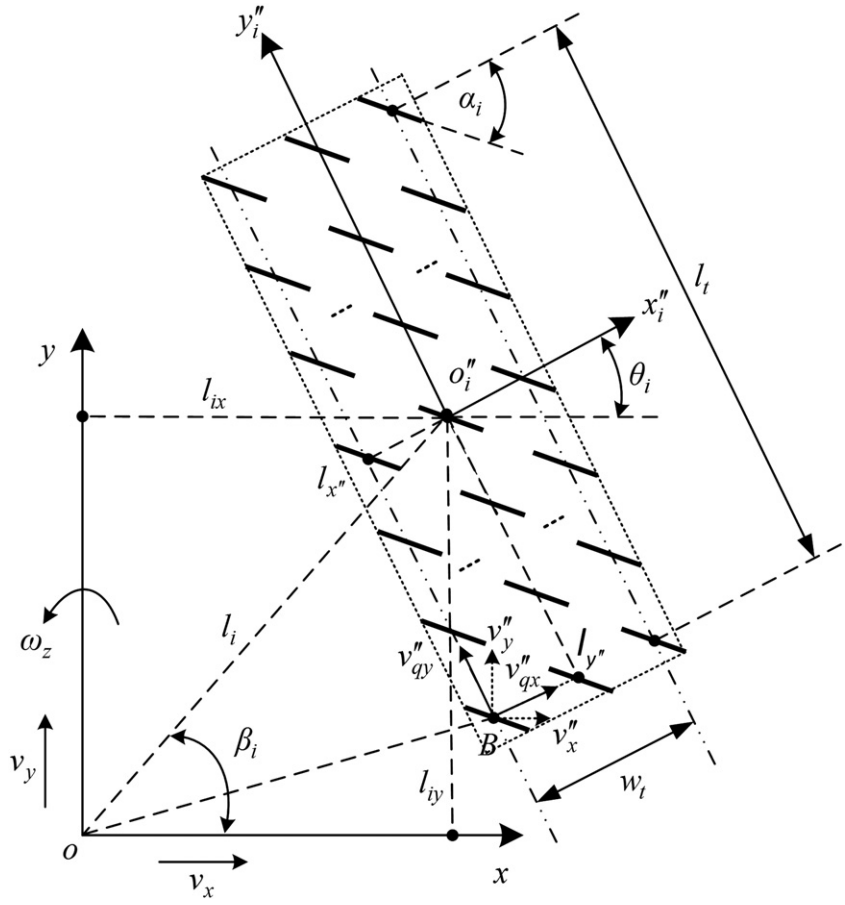

Fig. 5. Illustration of the velocity relation between the number *i* track and the vehicle.

Also, define the mean angular velocity of the driving sprocket as $\overline{\omega}_i$, and the mean relative velocity perpendicular to axes of the rollers as $\overline{v}_{ri}$. According to the mean value theorem of integrals, and combining Eqs. (8), (9), and (10), we have:

$$\begin{pmatrix} \overline{\omega}_i \\ \overline{v}_{ri} \end{pmatrix} = \begin{pmatrix} \dfrac{\sin(\theta_i+\alpha_i)}{r\sin\alpha_i} & \dfrac{\cos(\theta_i+\alpha_i)}{r\sin\alpha_i} & \dfrac{\int_{-\frac{l_t}{2}}^{\frac{l_t}{2}}\int_{-\frac{w_t}{2}}^{\frac{w_t}{2}} f_i\left(l_{x''},l_{y''}\right)dl_{x''}dl_{y''}}{\left(\frac{l_t}{2}-\left(-\frac{l_t}{2}\right)\right)\left(\frac{w_t}{2}-\left(-\frac{w_t}{2}\right)\right)} \\ \dfrac{\sin\theta_i}{\sin\alpha_i} & \dfrac{\cos\theta_i}{\sin\alpha_i} & \dfrac{\int_{-\frac{l_t}{2}}^{\frac{l_t}{2}}\int_{-\frac{w_t}{2}}^{\frac{w_t}{2}} g_i\left(l_{x''},l_{y''}\right)dl_{x''}dl_{y''}}{\left(\frac{l_t}{2}-\left(-\frac{l_t}{2}\right)\right)\left(\frac{w_t}{2}-\left(-\frac{w_t}{2}\right)\right)} \end{pmatrix} \begin{pmatrix} v_y \\ v_x \\ \omega_z \end{pmatrix}. \tag{11}$$

Hence, the general inverse kinematical equation of a vehicle equipped with omni-tracks is given by:

$$\begin{cases} \left(\overline{\omega}_1 \quad \overline{\omega}_2 \quad \cdots \quad \overline{\omega}_i \quad \cdots \quad \overline{\omega}_n\right)^{\mathrm{T}} = \boldsymbol{J}\left(v_y \quad v_x \quad v_z\right)^{\mathrm{T}} \\ \boldsymbol{J} = \dfrac{1}{r}\begin{pmatrix} \dfrac{\sin(\theta_1+\alpha_1)}{\sin\alpha_1} & \dfrac{\cos(\theta_1+\alpha_1)}{\cos\alpha_1} & \dfrac{\int_{-\frac{l_t}{2}}^{\frac{l_t}{2}}\int_{-\frac{w_t}{2}}^{\frac{w_t}{2}} f_1\left(l_{x''},l_{y''}\right)dl_{x''}dl_{y''}}{\left(\frac{l_t}{2}-\left(-\frac{l_t}{2}\right)\right)\left(\frac{w_t}{2}-\left(\frac{w_t}{2}\right)\right)} \\ \dfrac{\sin(\theta_2+\alpha_2)}{\sin\alpha_2} & \dfrac{\cos(\theta_2+\alpha_2)}{\cos\alpha_2} & \dfrac{\int_{-\frac{l_t}{2}}^{\frac{l_t}{2}}\int_{-\frac{w_t}{2}}^{\frac{w_t}{2}} f_2\left(l_{x''},l_{y''}\right)dl_{x''}dl_{y''}}{\left(\frac{l_t}{2}-\left(-\frac{l_t}{2}\right)\right)\left(\frac{w_t}{2}-\left(\frac{w_t}{2}\right)\right)} \\ \vdots & \vdots & \vdots \\ \dfrac{\sin(\theta_i+\alpha_i)}{\sin\alpha_i} & \dfrac{\cos(\theta_i+\alpha_i)}{\cos\alpha_i} & \dfrac{\int_{-\frac{l_t}{2}}^{\frac{l_t}{2}}\int_{-\frac{w_t}{2}}^{\frac{w_t}{2}} f_i\left(l_{x''},l_{y''}\right)dl_{x''}dl_{y''}}{\left(\frac{l_t}{2}-\left(-\frac{l_t}{2}\right)\right)\left(\frac{w_t}{2}-\left(\frac{w_t}{2}\right)\right)} \\ \vdots & \vdots & \vdots \\ \dfrac{\sin(\theta_n+\alpha_n)}{\sin\alpha_n} & \dfrac{\cos(\theta_n+\alpha_n)}{\cos\alpha_n} & \dfrac{\int_{-\frac{l_t}{2}}^{\frac{l_t}{2}}\int_{-\frac{w_t}{2}}^{\frac{w_t}{2}} f_n\left(l_{x''},l_{y''}\right)dl_{x''}dl_{y''}}{\left(\frac{l_t}{2}-\left(-\frac{l_t}{2}\right)\right)\left(\frac{w_t}{2}-\left(\frac{w_t}{2}\right)\right)} \end{pmatrix} \\ \begin{pmatrix} \overline{v}_{r1} \\ \overline{v}_{r2} \\ \vdots \\ \overline{v}_{ri} \\ \vdots \\ \overline{v}_{rn} \end{pmatrix} = \begin{pmatrix} \dfrac{\sin\theta_1}{\sin\alpha_1} & \dfrac{\cos\theta_1}{\sin\alpha_1} & \dfrac{\int_{-\frac{l_t}{2}}^{\frac{l_t}{2}}\int_{-\frac{w_t}{2}}^{\frac{w_t}{2}} g_1\left(l_{x''},l_{y''}\right)dl_{x''}dl_{y''}}{\left(\frac{l_t}{2}-\left(-\frac{l_t}{2}\right)\right)\left(\frac{w_t}{2}-\left(\frac{w_t}{2}\right)\right)} \\ \dfrac{\sin\theta_2}{\sin\alpha_2} & \dfrac{\cos\theta_2}{\sin\alpha_2} & \dfrac{\int_{-\frac{l_t}{2}}^{\frac{l_t}{2}}\int_{-\frac{w_t}{2}}^{\frac{w_t}{2}} g_2\left(l_{x''},l_{y''}\right)dl_{x''}dl_{y''}}{\left(\frac{l_t}{2}-\left(-\frac{l_t}{2}\right)\right)\left(\frac{w_t}{2}-\left(\frac{w_t}{2}\right)\right)} \\ \vdots & \vdots & \vdots \\ \dfrac{\sin\theta_i}{\sin\alpha_i} & \dfrac{\cos\theta_i}{\sin\alpha_i} & \dfrac{\int_{-\frac{l_t}{2}}^{\frac{l_t}{2}}\int_{-\frac{w_t}{2}}^{\frac{w_t}{2}} g_i\left(l_{x''},l_{y''}\right)dl_{x''}dl_{y''}}{\left(\frac{l_t}{2}-\left(-\frac{l_t}{2}\right)\right)\left(\frac{w_t}{2}-\left(\frac{w_t}{2}\right)\right)} \\ \vdots & \vdots & \vdots \\ \dfrac{\sin\theta_n}{\sin\alpha_n} & \dfrac{\cos\theta_n}{\sin\alpha_n} & \dfrac{\int_{-\frac{l_t}{2}}^{\frac{l_t}{2}}\int_{-\frac{w_t}{2}}^{\frac{w_t}{2}} g_n\left(l_{x''},l_{y''}\right)dl_{x''}dl_{y''}}{\left(\frac{l_t}{2}-\left(-\frac{l_t}{2}\right)\right)\left(\frac{w_t}{2}-\left(\frac{w_t}{2}\right)\right)} \end{pmatrix} \begin{pmatrix} v_y \\ v_x \\ \omega_z \end{pmatrix}. \end{cases} \tag{12}$$

The Eq. (11) is equivalent to:

$$\begin{pmatrix} \overline{\omega}_i \\ \overline{v}_{ri} \end{pmatrix} = \begin{pmatrix} \frac{\sin(\theta_i+\alpha_i)}{r\sin\alpha_i} & \frac{\cos(\theta_i+\alpha_i)}{r\sin\alpha_i} & \frac{l_{ix}\sin(\theta_i+\alpha_i)-l_{iy}\cos(\theta_i+\alpha_i)}{r\sin\alpha_i} \\ \frac{\sin\theta_i}{\sin\alpha_i} & \frac{\cos\theta_i}{\sin\alpha_i} & \frac{l_{ix}\sin\theta_i-l_{iy}\cos\theta_i}{\sin\alpha_i} \end{pmatrix} \begin{pmatrix} v_y \\ v_x \\ \omega_z \end{pmatrix}. \tag{13}$$

Assuming that Eq. (8) is equivalent to Eq. (13), we have $l_{x''} = l_{y''} = 0$, hence,

$$\begin{pmatrix} \overline{\omega}_i \\ \overline{v}_{ri} \end{pmatrix} = \begin{pmatrix} \omega_i \\ v_{ri} \end{pmatrix} \tag{14}$$

where ω_i is the angular velocity of the driving sprocket and v_{ri} is the relative velocity both based on the geometrical center point o''_i. Hence, each omni-track is equivalent to its geometrical center point.

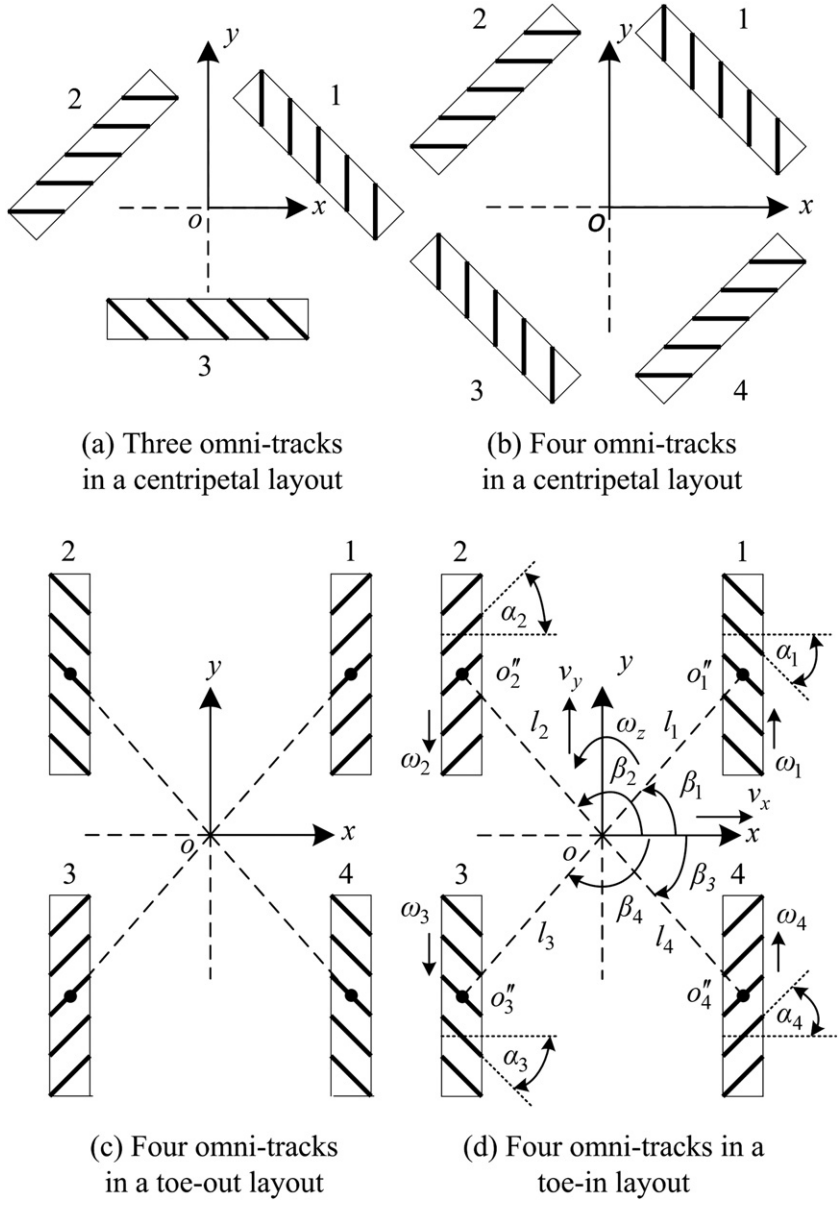

Fig. 6. Basic construction of the tracked-omni-vehicle (top view).

According to Fig. 5,

$$\begin{cases} l_{ix} = l_i \cos\beta_i \\ l_{iy} = l_i \sin\beta_i \end{cases}. \tag{15}$$

Combining Eqs. (12), (13), (14), and (15), the general inverse kinematical equation is equivalent to:

$$\begin{cases} (\omega_1 \quad \omega_2 \quad \cdots \quad \omega_n)^{\mathrm{T}} = \boldsymbol{J}(v_y \quad v_x \quad v_z)^{\mathrm{T}} \\ \boldsymbol{J} = \dfrac{1}{r}\begin{pmatrix} \frac{\sin\eta_1}{\sin\alpha_1} & \frac{\cos\eta_1}{\sin\alpha_1} & \frac{l_1\sin(\eta_1-\beta_1)}{\sin\alpha_1} \\ \frac{\sin\eta_2}{\sin\alpha_2} & \frac{\cos\eta_2}{\sin\alpha_2} & \frac{l_2\sin(\eta_2-\beta_2)}{\sin\alpha_2} \\ \vdots & \vdots & \vdots \\ \frac{\sin\eta_i}{\sin\alpha_i} & \frac{\cos\eta_i}{\sin\alpha_i} & \frac{l_i\sin(\eta_i-\beta_i)}{\sin\alpha_i} \\ \vdots & \vdots & \vdots \\ \frac{\sin\eta_n}{\sin\alpha_n} & \frac{\cos\eta_n}{\sin\alpha_n} & \frac{l_n\sin(\eta_n-\beta_n)}{\sin\alpha_n} \end{pmatrix} \\ \begin{pmatrix} v_{r1} \\ v_{r2} \\ \vdots \\ v_{rn} \end{pmatrix} = \begin{pmatrix} \frac{\sin\theta_1}{\sin\alpha_1} & \frac{\cos\theta_1}{\sin\alpha_1} & \frac{l_1\sin(\theta_1-\beta_1)}{\sin\alpha_1} \\ \frac{\sin\theta_2}{\sin\alpha_2} & \frac{\cos\theta_2}{\sin\alpha_2} & \frac{l_2\sin(\theta_2-\beta_2)}{\sin\alpha_2} \\ \vdots & \vdots & \vdots \\ \frac{\sin\theta_i}{\sin\alpha_i} & \frac{\cos\theta_i}{\sin\alpha_i} & \frac{l_i\sin(\theta_i-\beta_i)}{\sin\alpha_i} \\ \vdots & \vdots & \vdots \\ \frac{\sin\theta_n}{\sin\alpha_n} & \frac{\cos\theta_n}{\sin\alpha_n} & \frac{l_n\sin(\theta_n-\beta_n)}{\sin\alpha_n} \end{pmatrix} \begin{pmatrix} v_y \\ v_x \\ \omega_z \end{pmatrix} \end{cases} \tag{16}$$

where $\eta_i = \theta_i + \alpha_i$.

Because ω_i is the only input variable, $\boldsymbol{J}$ is the Jacobian matrix. According to the linear algebra theory, the column rank of a matrix is equal to its row rank. When the number of tracks is two, the row rank of $\boldsymbol{J}$ must be no more than two, so its column rank is also no more than two. In order to meet the essential condition, the number of tracks should be no less than three. Additionally, the vehicle construction also determines whether the column-rank of $\boldsymbol{J}$ can be equal to 3. When the number of tracks is three, there is one possible construction with a centripetal layout as shown in Fig. 6(a), but it is unsuitable for cross-country running. When the number of tracks is four, there are three possible kinds of construction. Equally, the construction with four omni-tracks in a centripetal layout as shown in Fig. 6(b), is also unsuitable for cross-country running. Although the construction with four omni-tracks in the longitudinal symmetrical toe-out layout as shown in Fig. 6(c), is suitable for cross-country running, it is difficult to achieve center-point steering, and in some cases cannot achieve it at all. Therefore, the construction with four omni-tracks in the longitudinal symmetrical toe-in layout as shown in Fig. 6(d), which is optimal, is applied to the tracked-omni-vehicle.

Also define l as the distance value, where $l_1 = l_2 = l_3 = l_4 = l$, γ the absolute value of the four offset angles, where $-\alpha_1 = \alpha_2 = -\alpha_3 = \alpha_4 = \gamma$ and $0 < \gamma < \pi/2$, β as the absolute value of the four distribution angles, where $\beta_1 = \beta, \beta_2 = \pi - \beta, \beta_3 = \beta - \pi$, $\beta_4 = -\beta$, and $0 < \beta < \pi/2$, and ρ as the radius value, where $r_1 = r_2 = r_3 = r_4 = \rho$.

According to Fig. 6(d), $\theta_1 = \theta_4 = 0$ and $\theta_2 = \theta_3 = \pi$.

Combined with Eq. (16), the inverse kinematical equation of the tracked-omni-vehicle is given by:

$$\begin{cases} \begin{pmatrix} \omega_1 \\ \omega_2 \\ \omega_3 \\ \omega_4 \end{pmatrix} = \dfrac{-1}{\rho\sin\gamma}\begin{pmatrix} -\sin\gamma & \cos\gamma & -l\sin(\gamma+\beta) \\ \sin\gamma & \cos\gamma & -l\sin(\gamma+\beta) \\ \sin\gamma & -\cos\gamma & -l\sin(\gamma+\beta) \\ -\sin\gamma & -\cos\gamma & -l\sin(\gamma+\beta) \end{pmatrix}\begin{pmatrix} v_y \\ v_x \\ \omega_z \end{pmatrix} = \boldsymbol{J}\begin{pmatrix} v_y \\ v_x \\ \omega_z \end{pmatrix} \\ \begin{pmatrix} v_{r1} \\ v_{r2} \\ v_{r3} \\ v_{r4} \end{pmatrix} = \begin{pmatrix} 0 & \frac{1}{\sin\gamma} & \frac{-l\sin\beta}{\sin\gamma} \\ 0 & \frac{-1}{\sin\gamma} & \frac{l\sin\beta}{\sin\gamma} \\ 0 & \frac{-1}{\sin\gamma} & \frac{-l\sin\beta}{\sin\gamma} \\ 0 & \frac{1}{\sin\gamma} & \frac{l\sin\beta}{\sin\gamma} \end{pmatrix}\begin{pmatrix} v_y \\ v_x \\ \omega_z \end{pmatrix} \end{cases} \tag{17}$$

where $rank\ (\boldsymbol{J}) = 3$.

2.2.3. Steering slip analysis of the tracked-omni-vehicle

For conventional tracked vehicles, the length vectors from each ground contact point to the steering center are different, so the following velocity vectors of different ground contact points of the same track are different. However, their relative (winding) velocity vectors are the same, theoretically. Therefore, their absolute velocity vectors are different and not all zeros. It is inevitable that there are lateral slippages in steering motion. Due to the slippages, there is great lateral resistance, which is a major factor in the poor steering performance of conventional tracked vehicles.

For the tracked-omni-vehicle, since the rollers are independent and can rotate freely, the relative velocity vectors of different ground contact points of different rollers can be different, but those of the same roller are still same. Assume that the normal load exerted on each roller is uniformly distributed, so define the geometrical center of its ground contact segment as its base point. Generally, the length of a roller is comparatively short, so the slippages of its other points that are relative to its base point can be ignored. There is no slippage on the geometrical center point of the omni-track theoretically, so it is inevitable that there are different slippages on the base points of different rollers in a steering motion. Because the rollers can rotate independently in directions perpendicular to their axes, these slippages concentrate in directions parallel to their axes. Assuming that the vehicle's normal load is uniformly distributed, define the coefficient of sliding friction as μ, and the vehicle's gravity as G. To compare with an equivalent conventional tracked vehicle, we define a “new concept” the steering slip-power ratio ξ, as follows:

$$\xi = \frac{P}{P'} = \frac{\mu G\overline{|v_{\mathbf{f}}|}}{\mu G\overline{\left|v'_f\right|}} = \frac{\overline{v_f}}{\overline{\left|v'_f\right|}} \tag{18}$$

where P and P' are respectively the steering slip-power of the tracked-omni-vehicle and an equivalent conventional tracked vehicle, and $\overline{|v_f|}$ and $\overline{\left|v'_f\right|}$ are the mean slip velocities.

Assuming that the omni-track is equipped with multi-columned rollers and considering a center-point steering motion, the steering slip velocity of any ground contact point was analyzed as shown in Fig. 7.

In the figure, point O is the geometrical center of the tracked-omni-vehicle, point A is the geometrical center point of the omni-track, and point B is any ground contact point. Additionally, XOY is the vehicle's and global coordinate, $x''o''y''$ is the coordinate of point A, $x'''o'''y'''$ is the coordinate of point B, the y''' axis is parallel to the axis of the roller, and τ is the included angle between $o''x''$ and $o''o'''$.

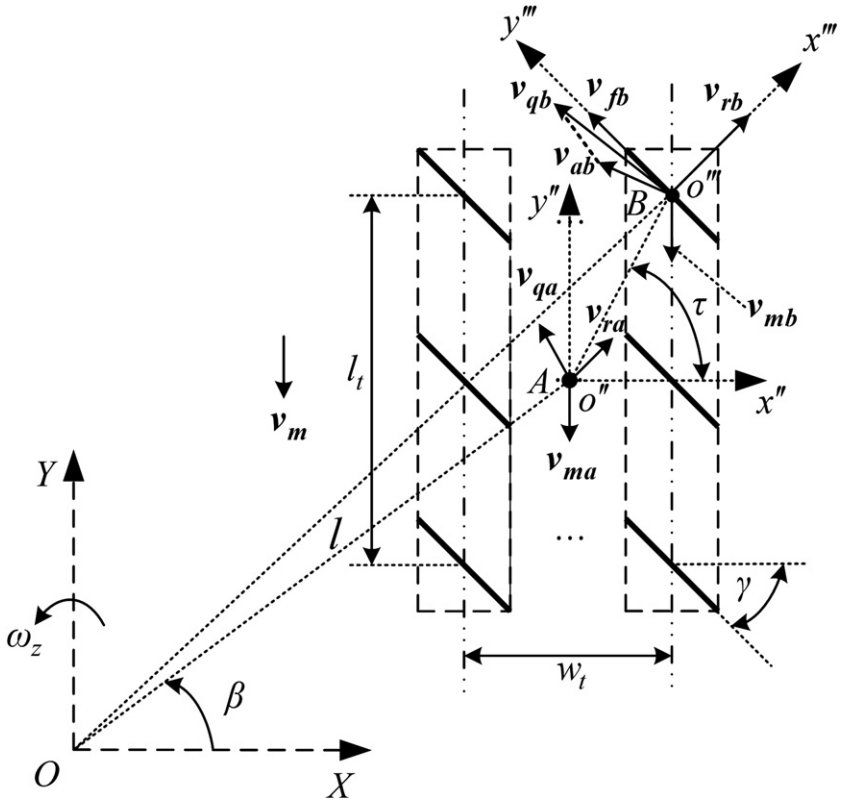

Fig. 7. Illustration of the steering slip velocity of any ground contact point.

The following velocity vectors of points A and B are respectively:

$$\boldsymbol{v}_{qa} = \omega_z \times \boldsymbol{OA} \tag{19}$$

where $|\boldsymbol{OA}| = l$.

$$\boldsymbol{v}_{qb} = \omega_z \times \boldsymbol{OB}. \tag{20}$$

Combining Eqs. (19) and (20):

$$\boldsymbol{v}_{qb} = \boldsymbol{v}_{qa} + \boldsymbol{v}_{ab} \tag{21}$$

where $\boldsymbol{v}_{ab} = \omega_z \times \boldsymbol{AB}$.

It is known that the absolute velocity vector of point A is:

$$\boldsymbol{v}_{fa} = \boldsymbol{v}_{qa} + \boldsymbol{v}_{ma} + \boldsymbol{v}_{ra} = 0. \tag{22}$$

The absolute velocity vector of point B is:

$$\boldsymbol{v}_{fb} = \boldsymbol{v}_{qb} + \boldsymbol{v}_{mb} + \boldsymbol{v}_{rb}. \tag{23}$$

And $\boldsymbol{v}_{fb}$ is in the direction parallel to the y''' axis, hence:

$$\boldsymbol{v}_{fb} = \boldsymbol{v}_{qby'''} + \boldsymbol{v}_{mby'''} + \boldsymbol{v}_{rby'''}. \tag{24}$$

Combining Eqs. (21) and (24):

$$\boldsymbol{v}_{fb} = \boldsymbol{v}_{qay'''} + \boldsymbol{v}_{aby'''} + \boldsymbol{v}_{mby'''} + \boldsymbol{v}_{rby'''}. \tag{25}$$

It is also known that:

$$\boldsymbol{v}_{ma} = \boldsymbol{v}_{mb} = \boldsymbol{v}_m \tag{26}$$

and

$$\boldsymbol{v}_{ray'''} = \boldsymbol{v}_{rby'''} = 0. \tag{27}$$

Combining Eqs. (25), (26), and (27):

$$\boldsymbol{v}_{fb} = \boldsymbol{v}_{qay'''} + \boldsymbol{v}_{aby'''} + \boldsymbol{v}_{may'''}. \tag{28}$$

Combining Eqs. (22), (27), and (28):

$$\boldsymbol{v}_{fb} = \boldsymbol{v}_{aby'''}. \tag{29}$$

Combined Fig. 7:

$$\left|\boldsymbol{v}_{aby'''}\right| = |\boldsymbol{v}_{ab}| \times \cos(\tau + \gamma - \pi/2). \tag{30}$$

It is known that $(l_{x''} \quad l_{y''})$ is the position of point B in the $x''o''y''$ coordinate, then:

$$|\boldsymbol{AB}| \times \cos\tau = |l_{x''}| \tag{31}$$

and

$$|\boldsymbol{AB}| \times \sin\tau = \left|l_{y''}\right|. \tag{32}$$

Combining Eqs. (29), (30), (31), and (32):

$$\left|\boldsymbol{v}_{fb}\right| = \omega_z \times \left(\left|l_{y''}\right| \cos\gamma + |l_{x''}| \sin\gamma\right). \tag{33}$$

According to the mean value theorem of integrals:

$$\overline{\left|\boldsymbol{v}_{\boldsymbol{f}}\right|} = \iint \left|v_{fb}\right| dl_{x''} dl_{y''}. \tag{34}$$

According to Fig. 7:

$$\begin{cases} l_{y''} \in \left[-\dfrac{l_t}{2}, \dfrac{l_t}{2}\right] \\ l_{x''} \in \left[-\dfrac{w_t}{2}, \dfrac{w_t}{2}\right] \end{cases}. \tag{35}$$

Combining Eqs. (33), (34), and (35), the mean slip velocity of the omni-track is:

$$\overline{|\mathbf{v}_{\mathbf{f}}|} = \omega_z \times \left(\int_{-\frac{l_t}{2}}^{\frac{l_t}{2}} \left| l_{y''} \right| cos\,\gamma\, dl_{y''} + \int_{-\frac{w_t}{2}}^{\frac{lw}{2}} |l_{x''}| sin\,\gamma\, dl_{x''} \right) = \omega_z \times \left(\frac{l_t}{2} \cos\gamma + \frac{w_t}{2} \sin\gamma \right). \tag{36}$$

If all the rollers are locked, the omni-track will become an equivalent conventional track. Equally, its mean slip velocity is:

$$\overline{\left|\boldsymbol{v}'_{\boldsymbol{f}}\right|} = \omega_z \times \sqrt{(l \sin\beta)^2 + \left(\frac{w_t}{2}\right)^2}. \tag{37}$$

Hence, the steering slip-power ratio ξ is:

$$\xi = \frac{\dfrac{l_t}{2} cos\,\gamma + \dfrac{w_t}{2} sin\,\gamma}{\sqrt{(l \sin\beta)^2 + \left(\frac{w_t}{2}\right)^2}}. \tag{38}$$

And there is:

$$\begin{cases} l sin\,\beta > \dfrac{1}{2} l_t \\ l_t \gg w_t \end{cases}. \tag{39}$$

Hence:

$$\xi < cos\,\gamma < 1. \tag{40}$$

It is indicated that the steering slip-power consumption of the tracked-omni-vehicle is much lower than that of an equivalent conventional tracked vehicle, so the tracked-omni-vehicle has superior steering efficiency compared to an equivalent conventional tracked vehicle.

According to Eq. (38), it is known that the steering slip-power ratio is related to the structure dimensions of the omni-track. In order to further reduce the steering slippage, two design rules are summarized as follows: (1) Trying to reduce the length of the omni-track on the premise that the tracked-omni-vehicle can meet the load requirements. (2) The length of the omni-track is generally much larger than its width, so it is advisable to add the number of roller columns appropriately to increase the ground contact area.

2.3. Dynamics analysis of the tracked-omni-vehicle

The Mecanum wheel can be considered a special case of the omni-track; the above kinematical theory should be also applicable to a Mecanum wheeled omnidirectional vehicle with the same construction, but whose steering slip-power ratio is zero. However, there is a conventional claim that this type of vehicle has lower longitudinal motion efficiency than that of a common wheeled vehicle, because most researchers consider that the traction of each Mecanum wheel still concentrates in the direction parallel to the axis of its ground contact roller in the longitudinal motion [17]. We have found that this conventional claim is wrong. And a different law regarding traction about the tracked-omni-vehicle has been proposed: When ground contact rollers rotate, the traction of each omni-track consists of two components respectively both parallel and perpendicular to their axes; however, the rotational friction of the rollers is extremely low (approximately zero), so the traction concentrates in the parallel direction. However, when ground contact rollers do not rotate, the traction moves in the longitudinal direction just like a conventional track, rather than in the parallel direction.

Because of various velocity combinations of the four omni-tracks, each omni-track must be driven independently. It is difficult to achieve independent drive for a mechanical drive system, which is commonly used in conventional tracked vehicles, so an independent electric drive system has been developed.

Define the output driving force vector of a motor (through the reducer) as $\boldsymbol{f}$, which is given by the motor's mechanical equation as follows:

$$T - fr = I_\omega \dot{\omega} + C\omega \tag{41}$$

where T is the output torque of the motor (through the reducer), I_ω is the inertia moment of the motor, and C is the viscous damping coefficient.

According to the above law, the traction vector $\boldsymbol{f}'$ exerted on the omni-track consists of two components:

$$\boldsymbol{f}' = \boldsymbol{f_q} + \boldsymbol{f_t} \tag{42}$$

where $\boldsymbol{f_q}$ is the component traction vector in the direction parallel to the roller's axis and $\boldsymbol{f_t}$ is the component traction vector in the direction perpendicular to the roller's axis.

However, $\boldsymbol{f_t}$ is extremely small, unless the rollers have no rotations:

$$\begin{cases} v_{ri} = 0 \\ \omega_i \neq 0 \end{cases}. \tag{43}$$

Hence, there is:

$$\begin{cases} \boldsymbol{f_q} = \boldsymbol{f}\sin\gamma \\ \boldsymbol{f_t} = \boldsymbol{f}\cos\gamma \ (v_r = 0) \\ \boldsymbol{f_t} \approx 0 \quad (v_r \neq 0) \end{cases}. \tag{44}$$

According to Eq. (17), only when the velocity of the vehicle is:

$$(v_y \quad v_x \quad \omega_z)^{\mathrm{T}} = (v_y \quad 0 \quad 0)^{\mathrm{T}} \tag{45}$$

then:

$$(v_{r1} \quad v_{r2} \quad v_{r3} \quad v_{r4})^{\mathrm{T}} = (0 \quad 0 \quad 0 \quad 0)^{\mathrm{T}}. \tag{46}$$

Therefore, only when a longitudinal motion is performed, none of the rollers have rotations theoretically, and the traction vector $\boldsymbol{f}'$ is:

$$\boldsymbol{f}' = \boldsymbol{f}. \tag{47}$$

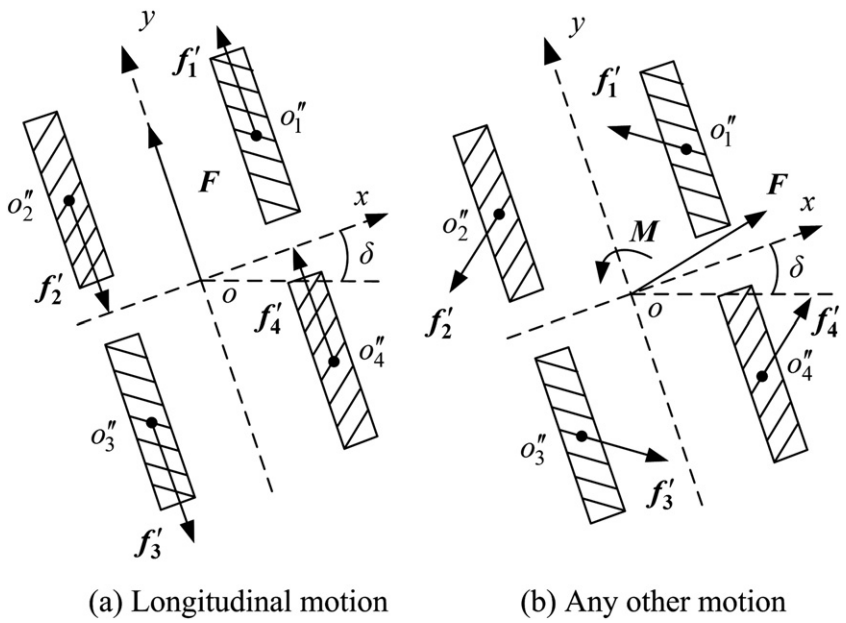

Fig. 8. Symbols for dynamics analysis of the tracked-omni-vehicle.

Otherwise,

$$\begin{cases} \boldsymbol{f}' = \boldsymbol{f_q} \\ \boldsymbol{f}' = \sin\gamma \end{cases}. \tag{48}$$

Fig. 8 shows symbols for dynamics analysis of the tracked-omni-vehicle on a plane. Assume that its center of gravity is coincident with its geometric center and its normal load is uniformly distributed.

Define $\dot{\boldsymbol{S}} = (\dot{\boldsymbol{x}} \quad \dot{\boldsymbol{y}})^{\mathrm{T}}$ as the translational velocity vector of the vehicle, $\ddot{\boldsymbol{S}} = (\ddot{\boldsymbol{x}} \quad \ddot{\boldsymbol{y}})^{\mathrm{T}}$ as the translational acceleration vector of the vehicle, $\dot{\boldsymbol{\delta}}$ as the angular velocity vector of the vehicle, $\ddot{\boldsymbol{\delta}}$ as the angular acceleration vector of the vehicle, $\boldsymbol{F} = (\boldsymbol{f_x} \quad \boldsymbol{f_y})^{\mathrm{T}}$ as the resultant traction vector exerted on the vehicle, $\boldsymbol{M}$ as the resultant traction moment vector exerted on the vehicle, m as the vehicle mass, and I_V as the inertia moment of the vehicle.

Firstly, analyze the longitudinal motion separately and the traction of each omni-track is in the longitudinal direction as shown in Fig. 8(a). To simplify the analysis, assume that the ground deformation resistance exerted on each track is extremely low and approximately zero. According to Newton's second law, the dynamical equation of the tracked-omni-vehicle in the longitudinal motion is given by:

$$m\ddot{y} = f_y \quad (\ddot{x} = 0 \quad \text{and} \quad \ddot{\delta} = 0) \tag{49}$$

where $\boldsymbol{f_y} = \boldsymbol{f_1'} - \boldsymbol{f_2'} - \boldsymbol{f_3'} + \boldsymbol{f_4'}$ and $f_1' = -f_2' = -f_3' = f_4'$.

Combining Eqs. (47) and (49):

$$m\ddot{y} = f_1 - f_2 - f_3 + f_4 \quad (\ddot{x} = 0 \quad \text{and} \quad \ddot{\delta} = 0). \tag{50}$$

Secondly, in any other motion, all the rollers generally have rotations, so the traction of each omni-track concentrates in the corresponding direction parallel to the axes of its ground contact rollers as shown in Fig. 8(b).

Equally, the dynamical equation of the tracked-omni-vehicle in other motions is given by:

$$\begin{cases} m\ddot{\boldsymbol{S}} = \boldsymbol{F} \\ I_V\ddot{\boldsymbol{\delta}} = \boldsymbol{M} \end{cases} \quad (\ddot{x} \neq 0 \quad \text{or} \quad \ddot{\delta} \neq 0). \tag{51}$$

Convert Eq. (51) to:

$$\begin{cases} m\left(\ddot{y} + \dot{x}\dot{\delta}\right) = f_y \\ m\left(\ddot{x} - \dot{y}\dot{\delta}\right) = f_x \\ \mathrm{I}_V\ddot{\delta} = M \end{cases} \quad (\ddot{x} \neq 0 \quad \text{or} \quad \ddot{\delta} \neq 0). \tag{52}$$

The parameters f_x, f_y, and M are given by:

$$\begin{cases} f_y = \sin\gamma(f_1' - f_2' - f_3' + f_4') \\ f_x = \cos\gamma(-f_1' - f_2' + f_3' + f_4') \\ M = l\sin(\gamma+\beta)(f_1' + f_2' + f_3' + f_4') \end{cases}. \tag{53}$$

Combining Eqs. (48) and (53):

$$\begin{cases} f_y = \sin\gamma(f_1 - f_2 - f_3 + f_4)\sin\gamma \\ f_x = \cos\gamma(-f_1 - f_2 + f_3 + f_4)\sin\gamma \\ M = l\sin(\gamma+\beta)(f_1 + f_2 + f_3 + f_4)\sin\gamma \end{cases}. \tag{54}$$

Combining Eq. (17), there is:

$$\begin{cases} r\omega_1 = \dot{y} - \dfrac{\cos\gamma}{\sin\gamma}\dot{x} + \dfrac{l\sin(\gamma+\beta)}{\sin\gamma}\dot{\delta} \\ r\omega_2 = -\dot{y} - \dfrac{\cos\gamma}{\sin\gamma}\dot{x} + \dfrac{l\sin(\gamma+\beta)}{\sin\gamma}\dot{\delta} \\ r\omega_3 = -\dot{y} + \dfrac{\cos\gamma}{\sin\gamma}\dot{x} + \dfrac{l\sin(\gamma+\beta)}{\sin\gamma}\dot{\delta} \\ r\omega_4 = \dot{y} + \dfrac{\cos\gamma}{\sin\gamma}\dot{x} + \dfrac{l\sin(\gamma+\beta)}{\sin\gamma}\dot{\delta} \end{cases}. \tag{55}$$

Combining Eqs. (41), (52), (54), and (55):

$$\begin{cases} \ddot{y} = a_1\,\dot{y} + a_2\,\dot{x}\dot{\delta} + b_1(T_1 - T_2 - T_3 + T_4) \\ \ddot{x} = a_3\,\dot{y}\dot{\phi} + a_4\,\dot{x} + b_2(T_3 + T_4 - T_1 - T_2) \quad (\ddot{x} \neq 0 \quad \text{or} \quad \ddot{\delta} \neq 0) \\ \ddot{\delta} = a_5\,\dot{\delta} + b_3(T_1 + T_2 + T_3 + T_4) \end{cases} \tag{56}$$

where $a_1 = \frac{-4C\sin^2\gamma}{mr^2+4I_\omega\sin^2\gamma}$, $a_2 = \frac{-mr^2}{mr^2+4I_\omega\sin^2\gamma}$, $b_1 = \frac{r\sin^2\gamma}{mr^2+4I_\omega\sin^2\gamma}$, $a_3 = \frac{mr^2}{mr^2+4I_\omega\cos^2\gamma}$, $a_4 = \frac{-4C\cos^2\gamma}{mr^2+4I_\omega\cos^2\gamma}$, $b_2 = \frac{r\sin\gamma\cos\gamma}{mr^2+4I_\omega\cos^2\gamma}$, $a_5 = \frac{-4Cl^2\sin^2(\gamma+\beta)}{I_V r^2+4I_\omega l^2\sin^2(\gamma+\beta)}$, and $b_3 = \frac{rl\sin(\gamma+\beta)\sin\gamma}{I_V r^2+4I_\omega l^2\sin^2(\gamma+\beta)}$.

Equally, combining Eqs. (41), (50), and (55):

$$\ddot{y} = a_1'\,\dot{y} + b_1'(T_1 - T_2 - T_3 + T_4) \quad \ddot{x} = 0 \quad \text{and} \quad \ddot{\delta} = 0 \tag{57}$$

where $a_1' = \frac{-4C}{mr^2+4I_\omega}$ and $b_1' = \frac{r}{mr^2+4I_\omega}$.

Setting $\begin{pmatrix} \dot{y} & \dot{x} & \dot{\delta} \end{pmatrix}^{\mathrm{T}}$ as the state vector, and $(T_1 \quad T_2 \quad T_3 \quad T_4)^{\mathrm{T}}$ as the input vector, the dynamic state space equation of the tracked-omni-vehicle is given by:

$$\begin{cases} \begin{pmatrix} \ddot{y} \\ \ddot{x} \\ \ddot{\delta} \end{pmatrix} = \begin{pmatrix} a_1 & a_2\,\dot{\delta} & 0 \\ a_3\,\dot{\delta} & a_4 & 0 \\ 0 & 0 & a_5 \end{pmatrix} \begin{pmatrix} \dot{y} \\ \dot{x} \\ \dot{\delta} \end{pmatrix} \\ + \begin{pmatrix} b_1 & -b_1 & -b_1 & b_1 \\ -b_2 & -b_2 & b_2 & b_2 \\ b_3 & b_3 & b_3 & b_3 \end{pmatrix} \begin{pmatrix} T_1 \\ T_2 \\ T_3 \\ T_4 \end{pmatrix} \quad (\ddot{x} \neq 0 \quad \text{or} \quad \ddot{\delta} \neq 0) \\ \begin{pmatrix} \ddot{y} \\ \ddot{x} \\ \ddot{\delta} \end{pmatrix} = \begin{pmatrix} a_1' & 0 & 0 \\ 0 & 0 & 0 \\ 0 & 0 & 0 \end{pmatrix} \begin{pmatrix} \dot{y} \\ \dot{x} \\ \dot{\delta} \end{pmatrix} \\ + \begin{pmatrix} b_1' & -b_1' & -b_1' & b_1' \\ 0 & 0 & 0 & 0 \\ 0 & 0 & 0 & 0 \end{pmatrix} \begin{pmatrix} T_1 \\ T_2 \\ T_3 \\ T_4 \end{pmatrix} \quad (\ddot{x} = 0 \quad \text{and} \quad \ddot{\delta} = 0) \end{cases} . \tag{58}$$

2.4. Anisotropy analysis of the tracked-omni-vehicle

Due to the offset angle, the maximum translational velocities that the tracked-omni-vehicle can reach are different when it moves in different directions, and its maximum translational accelerations are also different. This is called anisotropy [18]. Therefore, the relation of the offset angle and the anisotropy is analyzed, and the optimal offset angle is chosen.

Considering the maximum translational velocities and combined with Eq. (17), it is defined as:

$$r\omega_i = c_{i1}v_y + c_{i2}v_x + c_{i3}\omega_z \quad (i = 1, 2, 3, 4)\,. \tag{59}$$

When the tracked-omni-vehicle only performs translational motions on a plane, define V as the translational velocity of the vehicle, and σ as the translational direction angle, where $0° \le \sigma \le 360°$.Combining with Eq. (59):

$$r\omega_i = V(c_{i1}\sin\sigma + c_{i2}\cos\sigma). \tag{60}$$

Assume that $|r\omega_i| \le 1$,

$$|V| \le \frac{1}{|c_{i1}\sin\sigma + c_{i2}\cos\sigma|} \quad (|c_{i1}\sin\sigma + c_{i2}\cos\sigma| \neq 0)\,. \tag{61}$$

Then the maximum translational velocity is given by:

$$|V|_{max} = \frac{1}{|c_{i1}\sin\sigma + c_{i2}\cos\sigma|_{max}}\,. \tag{62}$$

Combined with Eq. (17):

$$(c_{i1} \quad c_{i2}) = \begin{pmatrix} 1 & -\dfrac{\cos\gamma}{\sin\gamma} \\ -1 & -\dfrac{\cos\gamma}{\sin\gamma} \\ -1 & \dfrac{\cos\gamma}{\sin\gamma} \\ 1 & \dfrac{\cos\gamma}{\sin\gamma} \end{pmatrix}. \tag{63}$$

According to Eq. (63):

$$|c_{i1}\sin\sigma + c_{i2}\cos\sigma|_{\max} = |\sin\sigma| + \left|\frac{\cos\gamma}{\sin\gamma}\cos\sigma\right|. \tag{64}$$

Combining Eqs. (62) and (64):

$$|V|_{max} = \frac{1}{|\sin\sigma| + \left|\dfrac{\cos\gamma}{\sin\gamma}\cos\sigma\right|}. \tag{65}$$

Considering four different offset angles, such as $\pi/12$, $\pi/6$, $\pi/4$, and $\pi/3$, the maximum translational velocities in all directions are plotted respectively as shown in Fig. 9.

There are the same maximum translational velocities in the directions of 90 and 270° (the longitudinal direction) for the four offset angles. Therefore, the maximum longitudinal translational velocities have no relation to the offset angle. However, there are different maximum translational velocities in the directions of 0 and 180° (the lateral direction), and the greater the offset angle is, the larger the maximum lateral translational velocities are. This is especially true when the offset angle is $\pi/4$; there are the same maximum translational velocities in the lateral direction as those in the longitudinal direction. The maximum translational velocities in other directions change accordingly with those in the longitudinal and lateral directions.

Consider the maximum translational accelerations and assume that the initial velocity of the tracked-omni-vehicle is:

$$\left(\dot{y} \quad \dot{x} \quad \dot{\delta}\right)^{\mathrm{T}} = (0 \quad 0 \quad 0)^{\mathrm{T}}. \tag{66}$$

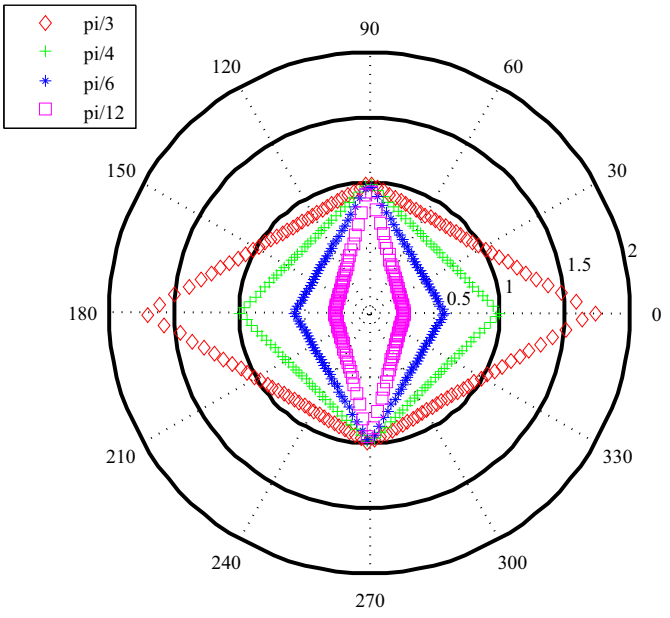

Fig. 9. Maximum translational velocities in all directions.

Combining Eqs. (58) and (66):

$$\begin{cases} \begin{pmatrix} \ddot{y} \\ \ddot{x} \\ \ddot{\delta} \end{pmatrix} = \begin{pmatrix} b_1 & -b_1 & -b_1 & b_1 \\ -b_2 & -b_2 & b_2 & b_2 \\ b_3 & b_3 & b_3 & b_3 \end{pmatrix} \begin{pmatrix} T_1 \\ T_2 \\ T_3 \\ T_4 \end{pmatrix} \\ = \boldsymbol{K} \begin{pmatrix} T_1 \\ T_2 \\ T_3 \\ T_4 \end{pmatrix} \quad (\ddot{x} \neq 0 \quad \text{or} \quad \ddot{\delta} \neq 0) \\ \begin{pmatrix} \ddot{y} \\ \ddot{x} \\ \ddot{\delta} \end{pmatrix} = \begin{pmatrix} b'_1 & -b'_1 & -b'_1 & b'_1 \\ 0 & 0 & 0 & 0 \\ 0 & 0 & 0 & 0 \end{pmatrix} \begin{pmatrix} T_1 \\ T_2 \\ T_3 \\ T_4 \end{pmatrix} \quad (\ddot{x} = 0 \quad \text{and} \quad \ddot{\delta} = 0) \end{cases} . \tag{67}$$

Hence, the inverse dynamical equation of the tracked-omni-vehicle is given by:

$$\begin{cases} \begin{pmatrix} T_1 \\ T_2 \\ T_3 \\ T_4 \end{pmatrix} = \begin{pmatrix} \frac{1}{4b_1} & -\frac{1}{4b_2} & \frac{1}{4b_3} \\ -\frac{1}{4b_1} & -\frac{1}{4b_2} & \frac{1}{4b_3} \\ -\frac{1}{4b_1} & \frac{1}{4b_2} & \frac{1}{4b_3} \\ \frac{1}{4b_1} & \frac{1}{4b_2} & \frac{1}{4b_3} \end{pmatrix} \begin{pmatrix} \ddot{y} \\ \ddot{x} \\ \ddot{\delta} \end{pmatrix} \\ = \boldsymbol{K}^{+} \begin{pmatrix} \ddot{y} \\ \ddot{x} \\ \ddot{\delta} \end{pmatrix} \quad (\ddot{x} \neq 0 \quad \text{or} \quad \ddot{\delta} \neq 0) \\ \begin{pmatrix} T_1 \\ T_2 \\ T_3 \\ T_4 \end{pmatrix} = \begin{pmatrix} \frac{1}{4b'_1} & 0 & 0 \\ -\frac{1}{4b'_1} & 0 & 0 \\ -\frac{1}{4b'_1} & 0 & 0 \\ \frac{1}{4b'_1} & 0 & 0 \end{pmatrix} \begin{pmatrix} \ddot{y} \\ \ddot{x} \\ \ddot{\delta} \end{pmatrix} \quad (\ddot{x} = 0 \quad \text{and} \quad \ddot{\delta} = 0) \end{cases} \tag{68}$$

where $\boldsymbol{K}^{+}$ is the generalized inverse matrix of $\boldsymbol{K}$, $\boldsymbol{K}^{+} = \boldsymbol{K}^{\mathrm{T}}(\boldsymbol{K}\boldsymbol{K}^{\mathrm{T}})^{-1}$.

When the tracked-omni-vehicle only performs translational motions on a plane, and combined with Eq. (68), it is defined as:

$$\begin{cases} T_i = d_{i1}\ddot{y} + d_{i2}\ddot{x} \quad (x \neq 0) \\ T_i = d'_{i1}\ddot{y} \quad (\ddot{x} = 0) \end{cases} \quad (i = 1, 2, 3, 4) . \tag{69}$$

It is known that:

$$\begin{cases} \ddot{y} = S\sin\sigma \\ \ddot{x} = S\cos\sigma \end{cases} . \tag{70}$$

Combining Eqs. (69) and (70):

$$\begin{cases} T_i = \ddot{S}(d_{i1}\sin\sigma + d_{i2}\cos\sigma) \quad (\sigma \neq 90, \quad 270^\circ) \\ T_i = d'_{i1}\ddot{S} \quad (\sigma = 90, \quad 270^\circ) \end{cases} . \tag{71}$$

Convert Eq. (71) to:

$$\begin{cases} \left|\ddot{S}\right| = \dfrac{|T_i|}{|d_{i1}\sin\sigma + d_{i2}\cos\sigma|} \quad (\sigma \neq 90, \quad 270^\circ) \\ \left|\ddot{S}\right| = \dfrac{|T_i|}{|d'_{i1}|} \quad (\sigma = 90, \quad 270^\circ) \end{cases} . \tag{72}$$

Assume that:

$$\frac{|T_i|}{mr} \leq 1. \tag{73}$$

Combining Eqs. (72) and (73):

$$\begin{cases} \left|\ddot{S}\right| \le \dfrac{mr}{\left|d_{i1}\sin\sigma + d_{i2}\cos\sigma\right|} & (\sigma \neq 90,\quad 270^\circ) \\ \left|\ddot{S}\right| \le \dfrac{mr}{\left|d'_{i1}\right|} & (\sigma = 90,\quad 270^\circ) \end{cases}. \tag{74}$$

Hence:

$$\begin{cases} \left|\ddot{S}\right|_{\max} = \dfrac{mr}{\left|d_{i1}\sin\sigma + d_{i2}\cos\right|_{\max}} & (\sigma \neq 90,\quad 270^\circ) \\ \left|\ddot{S}\right|_{\max} = \dfrac{mr}{\left|d'_{i1}\right|_{\max}} & (\sigma = 90,\quad 270^\circ) \end{cases}. \tag{75}$$

Combined with Eq. (68), there are:

$$\begin{cases} \left|d_{i1}\sin\sigma + d_{i2}\cos\right|_{\max} = \left|\dfrac{1}{4b_1}\sin\sigma\right| + \left|\dfrac{1}{4b_2}\cos\sigma\right| \\ \left|d'_1\right|_{\max} = \dfrac{1}{4b'_1} \end{cases}. \tag{76}$$

Define the motor mass as m', and it is known that:

$$m \gg m'. \tag{77}$$

Hence,

$$mr^2 \gg I_w. \tag{78}$$

To simplify the analysis, assume that:

$$I_w \approx 0. \tag{79}$$

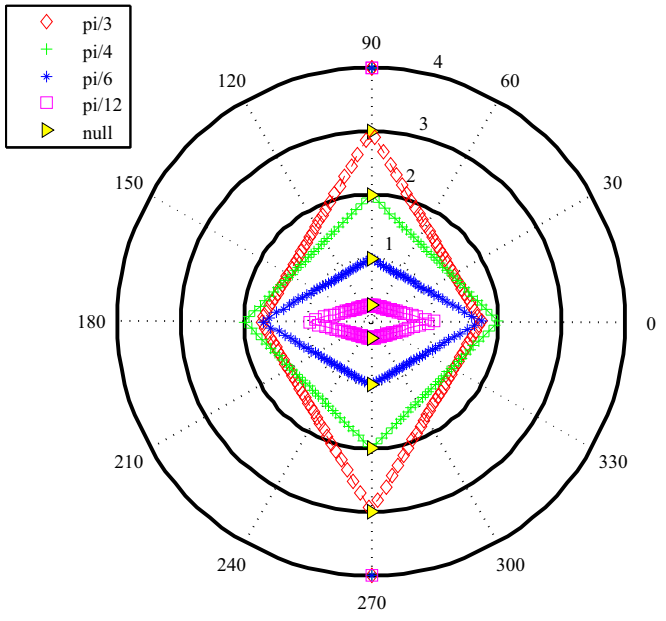

Fig. 10. Maximum translational accelerations in all directions.

Combining Eqs. (75), (76), and (79), the maximum translational acceleration is given by:

$$\begin{cases} \left|\ddot{S}\right|_{\max} = \dfrac{4\sin\gamma}{\left|\dfrac{1}{\sin\gamma}\sin\sigma\right| + \left|\dfrac{1}{\cos\gamma}\cos\sigma\right|} & (\sigma \neq 90,\quad 270^\circ) \\ \left|\ddot{S}\right|_{\max} = 4 \quad (\sigma = 90,\quad 270^\circ) \end{cases} . \tag{80}$$

Considering four different offset angles, such as $\pi/12$, $\pi/6$, $\pi/4$, and $\pi/3$, the maximum translational accelerations in all directions are plotted respectively as shown in Fig. 10.

There are the same maximum translational accelerations in the directions of 90 and 270° (the longitudinal direction) for these four offset angles, so the maximum longitudinal translational accelerations also have no relation to the offset angle. However, there are different maximum translational accelerations in the directions of 0 and 180° (the lateral direction). When the offset angle is $\pi/4$, the maximum translational accelerations in the lateral direction are the largest, which is half of that in the longitudinal direction, and the maximum translational accelerations in other directions are much more balanced than those with other offset angles. When the offset angle is smaller than $\pi/4$, the smaller the offset angle is, the smaller the maximum translational accelerations are, in any other direction except the longitudinal direction.

In summary, a conclusion has been reached: $\pi/4$ is the optimal offset angle, with which the tracked-omni-vehicle performs the most balanced anisotropy.

3. Experiments of the tracked-omni-vehicle

A prototype of the tracked-omni-vehicle has been manufactured as shown in Fig. 11. And the prototype's primary parameters are shown in Table 1. According to the inverse kinematical equation of the tracked-omni-vehicle, the omnidirectional motion can be achieved by different velocity combinations of the four omni-tracks, so each track must be driven independently. However, neither a mechanical drive system nor a hydraulic drive system is appropriate to the tracked-omni-vehicle, because it is difficult to realize independent drive for each track in a mechanical drive system and to possess high frequency response for actuators of a hydraulic drive system. Therefore, the prototype is equipped with an independent electric drive system as shown in Fig. 12. Each drive sprocket is connected to a brushless DC motor and its driver. The power is a lithium battery. The core of the drive system is the motion controller, which consists of a digital signal processor (DSP), and some peripheral interface circuits, including a CAN interface circuit, an A/D conversion circuit, a serial RS232 interface circuit, and multi-I/O interface circuits. The remote controller consists of a single chip microcomputer (SCM), some peripheral interface circuits, a triaxial joystick, a lithium battery, and a pair of wireless communication modules. Additionally, the independent suspensions are necessary to help with omnidirectional motion on uneven terrains, because they are conducive in keeping the four omni-tracks in contact with the ground simultaneously. And with consideration to the durability of the omni-track, only grease has been used for roller rotations instead of bearings.

The prototype's control architecture is shown in Fig. 13. In order to achieve accurate omnidirectional motion, the velocity control mode is more appropriate to the motors than the torque control mode. The control flow is as follows: Firstly, the voltage values of

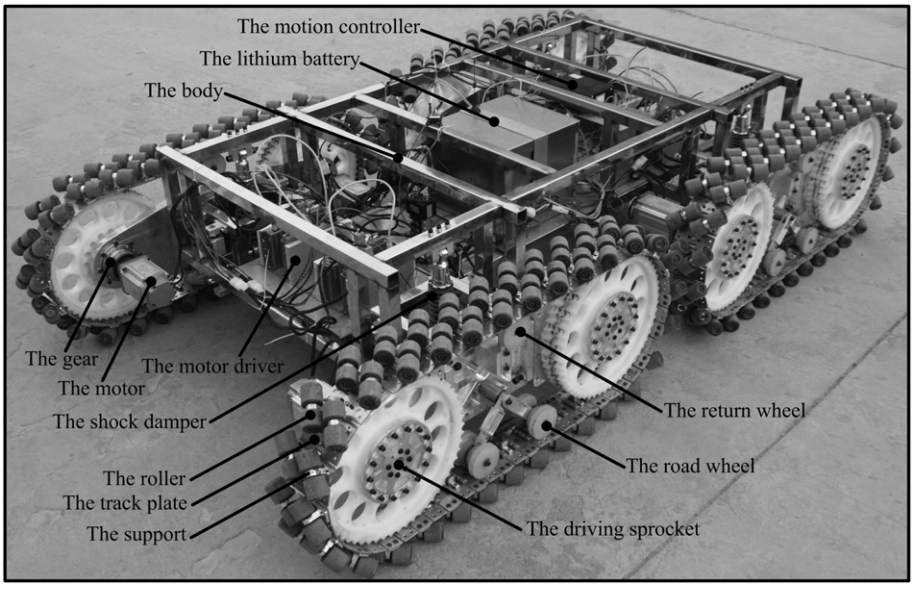

Fig. 11. Illustration of the prototype of the tracked-omni-vehicle.

Table 1
Primary parameters of the prototype.

No.	Items	Value
1	Length (m)	2.172
2	Width (m)	1.258
3	Offset angle (rad)	$\pi/4$
4	Track radius (m)	≈ 0.34
5	Roller radius (m)	0.019
6	Center distance l (m)	≈ 0.78
7	Distribution angle β (rad)	≈ 0.812
8	Length of the ground contact segment l_t (m)	≈ 0.64
9	Width of the ground contact segment w_t (m)	≈ 0.06
10	Maximum translational velocity (km/h)	≥ 7
11	Brushless DC motor (W)	440
12	Lithium battery	48 V 70 Ah

three axes of the joystick were converted to digital signals using an A/D conversion circuit in every sampling period; these values were immediately transmitted to the motion controller via the SCM over serial RS232. The remote controller and the motion controller were connected through the pair of 433 MHz wireless communication modules. When the DSP received these values, it solved the corresponding velocities of the four tracks based on the inverse kinematical equation of the tracked-omni-vehicle, then transferred the speed instructions to each motor driver over CAN.

In this section, we describe a set of experiments conducted to confirm the performance of the tracked-omni-vehicle.

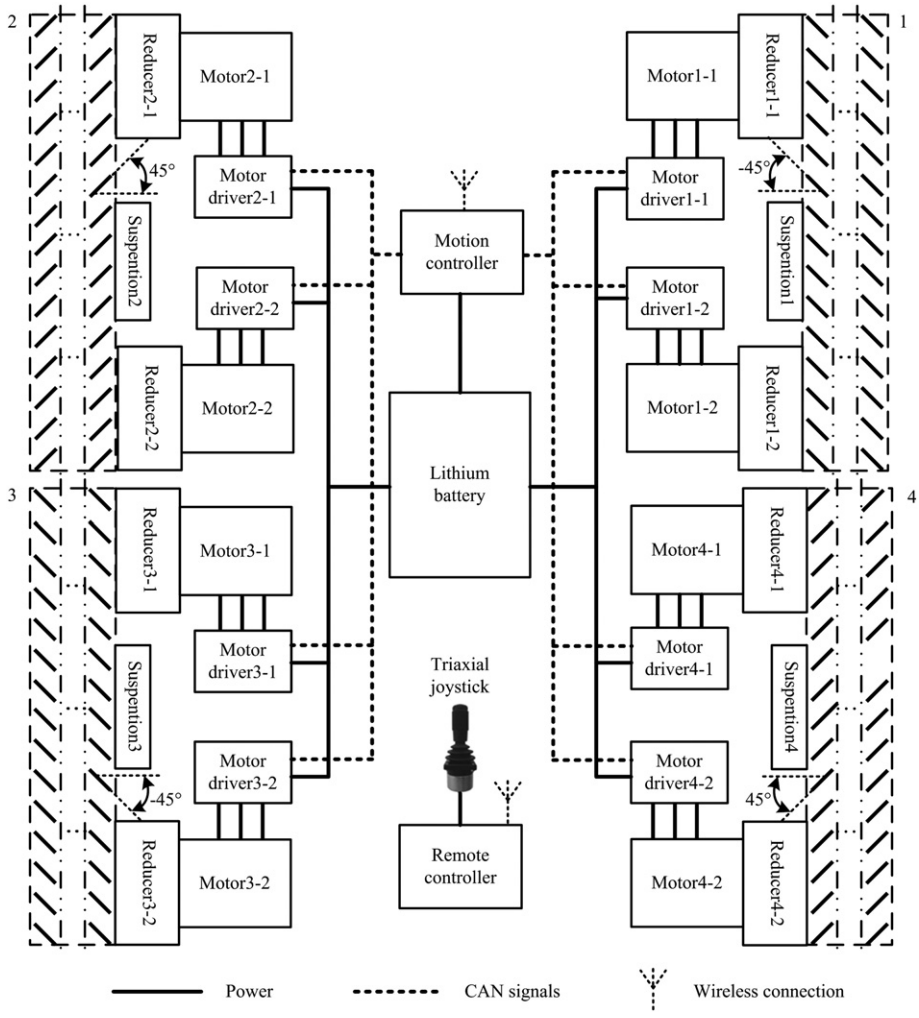

Fig. 12. Illustration of the independent electric driving system.

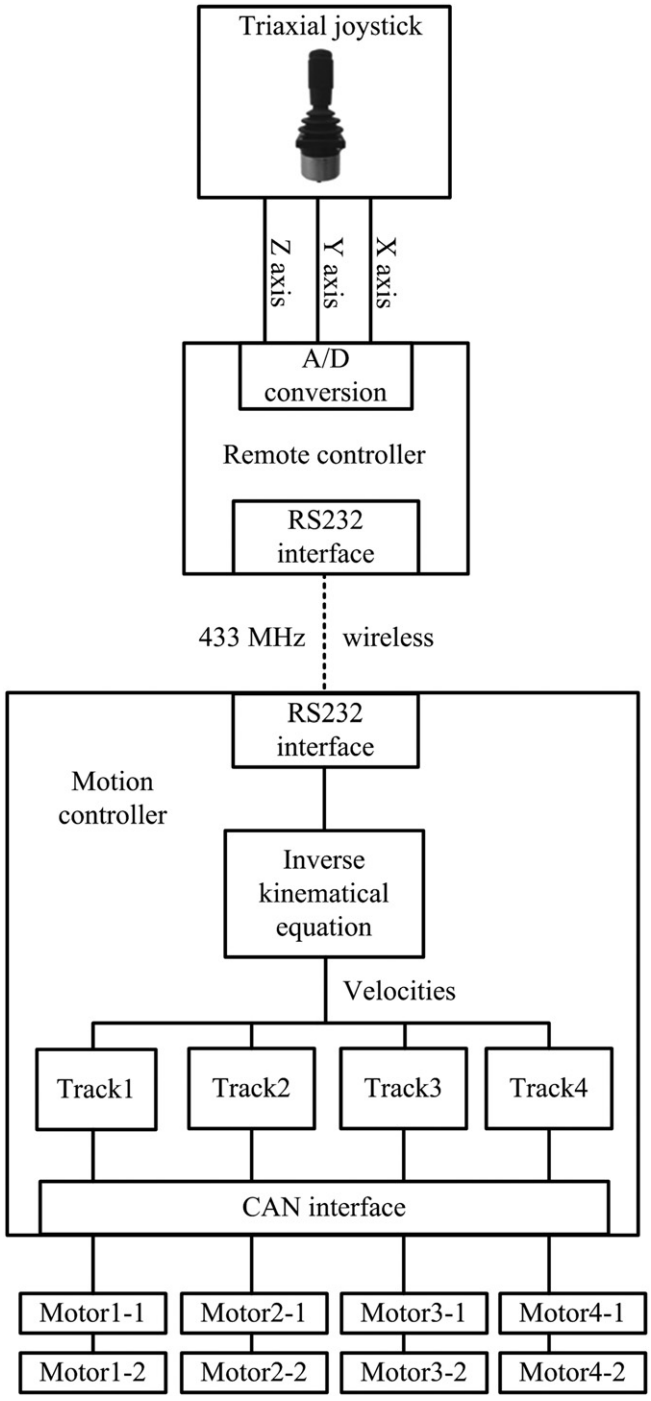

Fig. 13. Illustration of the prototype's control architecture.

3.1. Omnidirectional motion experiment

The prototype vehicle performed omnidirectional motion not only easily on flat terrain, but also effectively and stably on uneven terrains as shown in Fig. 14(a), (b), and (c). However, the vehicle had difficulty performing the lateral motion on ice as shown in Fig. 14(d), because the ice adhesion was too small to overcome the rotational friction of the rollers; without the rotation of the rollers, the prototype ran just like a conventional tracked vehicle on ice. In a word, terrain conditions vary, but the vehicle was able to achieve omnidirectional motion so long as the ground contact rollers were able to rotate.

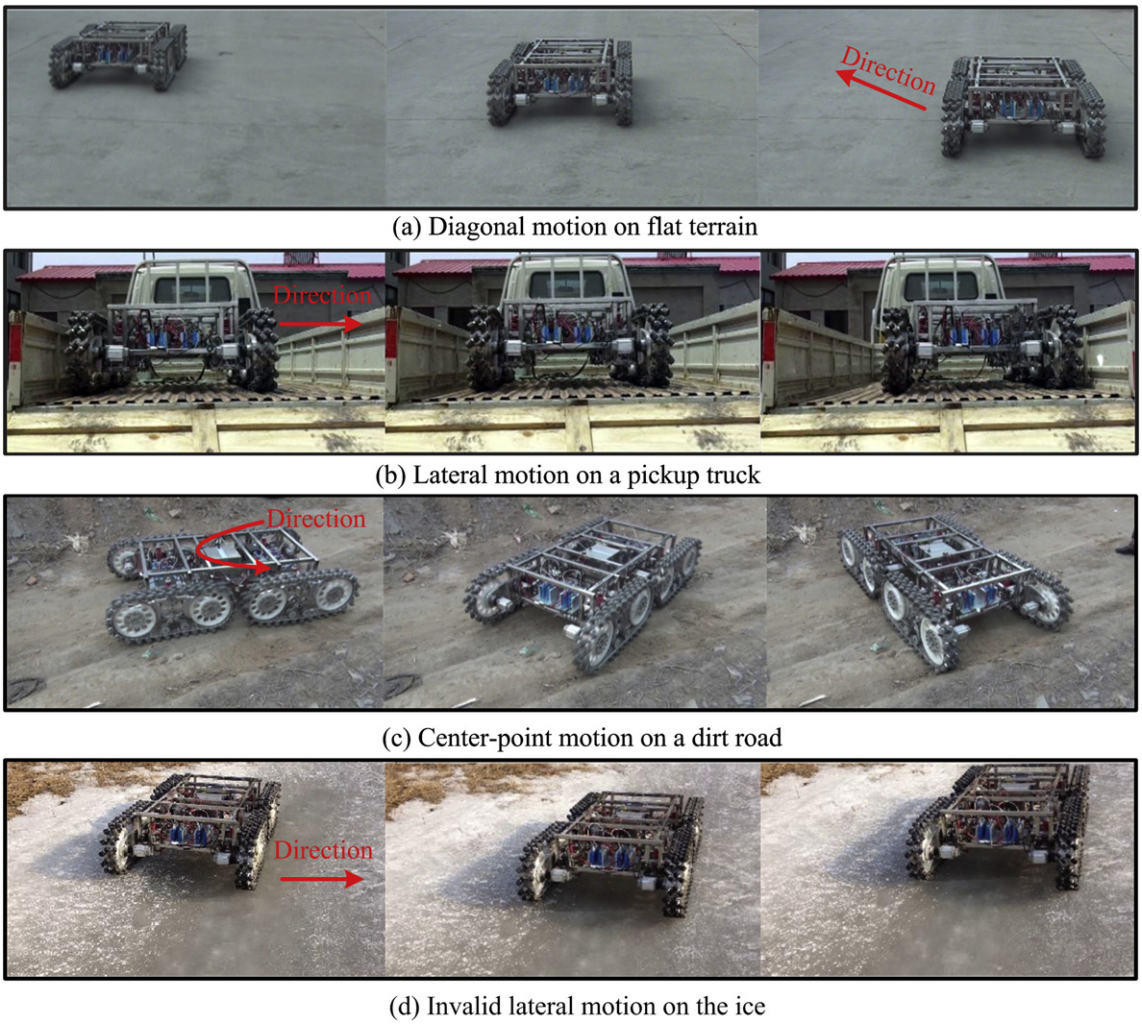

Fig. 14. Illustrations of omnidirectional motion on different terrains.

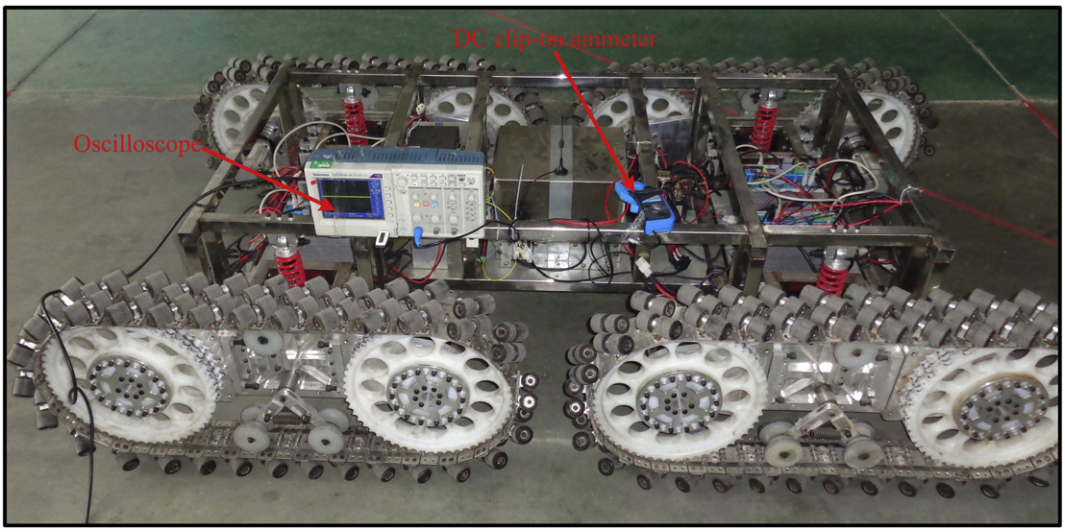

Fig. 15. The experiment's measuring instruments.

3.2. Steering motion efficiency experiment

According to the parameters of the prototype shown in Table 1 and combining with Eq. (38), the prototype's theoretical steering slip-power ratio is approximately 0.44. To simplify the experiments, the prototype was tested at a maximum steering angular velocity, and we set the maximum rotate speed of each motor as 4000 rpm. The prototype's total current (the battery's output current) was measured using a DC clip-on ammeter, which has two levels of precision, 1 mV/1 A and 100 mV/1 A. It is also connected to an oscilloscope as shown in Fig. 15, with which the total current is shown in real-time and can be saved. When the prototype remained at a steady maximum velocity, we measured the total current in a fixed period, and then recorded the mean total current shown in the oscilloscope.

Firstly, considering that the rollers' rolling resistance has been ignored in the theoretical analysis, we carried out this experiment on a flat surface. And the measuring result was shown in Fig. 16(a), the mean value of which was approximately 13.53 A.

Secondly, to compare the prototype with an equivalent conventional tracked vehicle, we locked all the rollers by adding a 2 mm thick washer between each roller and its support. In the same way, the "locked" vehicle's total current was measured as shown in Fig. 16(b), the mean value of which is approximately 28.93 A. Because the power consumption of the rollers' rotations and some other power consumption were much smaller than the slip power consumption, the actual steering slip-power ratio could be comparable to the total current ratio. And the actual steering slip-power ratio was approximately 0.47, which was close to the theoretical value. Consequently, it was demonstrated that the tracked-omni-vehicle has superior steering efficiency compared to that of an equivalent conventional tracked vehicle.

3.3. Longitudinal motion efficiency experiment

On the same flat surface, the prototype was tested at a maximum longitudinal velocity, and its total current was measured as shown in Fig. 17(a), the mean value of which was approximately 8.59 A. Additionally, it has been verified that the prototype's

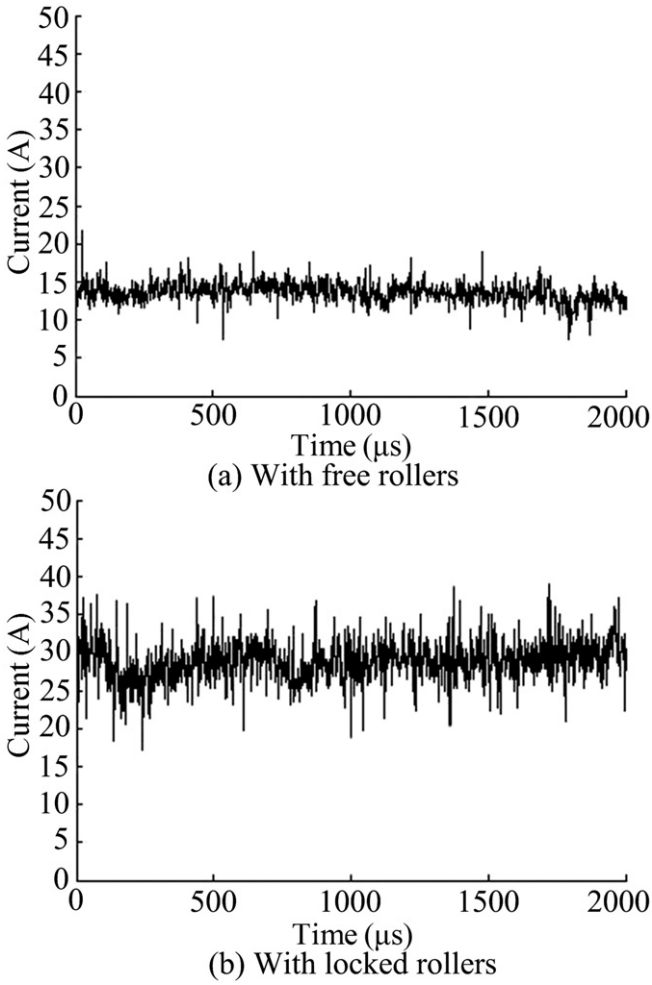

Fig. 16. Total current of center-point steering motion.

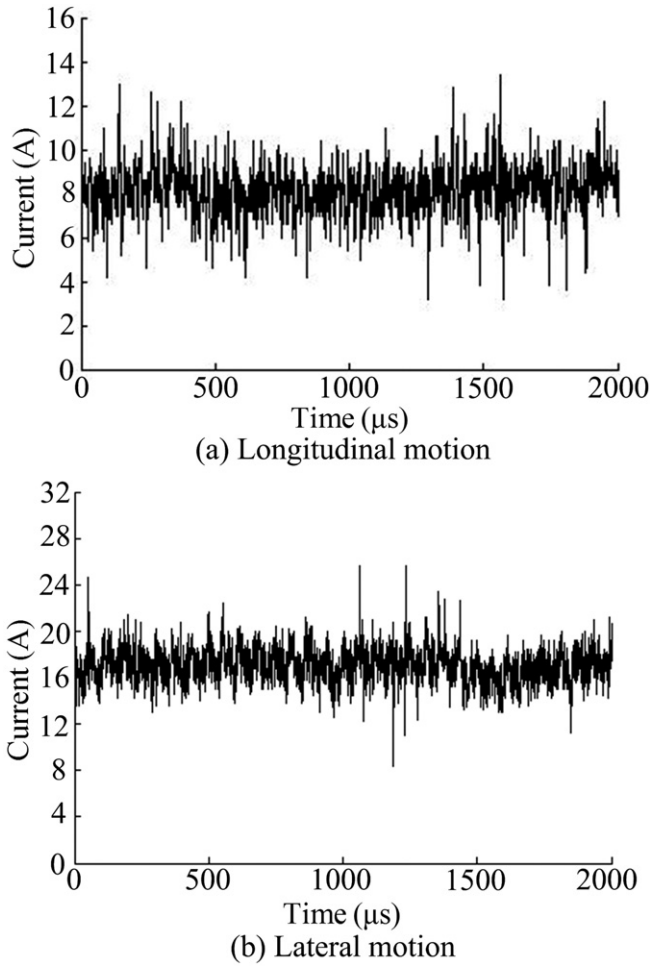

Fig. 17. Total current of longitudinal and lateral motion with free rollers.

maximum lateral velocity was equal to its maximum longitudinal velocity. Also, the mean value of the prototype's total current at a maximum lateral velocity was measured at approximately 17.05 A as shown in Fig. 17(b), which was about 2 times of that at a maximum longitudinal velocity. That is, the vehicle's lateral motion efficiency was half of its longitudinal motion efficiency, and it was verified that the anisotropy is right. For the "locked" vehicle, its total current at a maximum longitudinal motion was measured as shown in Fig. 18, the mean value of which was approximately 8.25 A. Consequently, it was demonstrated that the tracked-omni-vehicle has equal longitudinal motion efficiency to an equivalent conventional tracked vehicle.

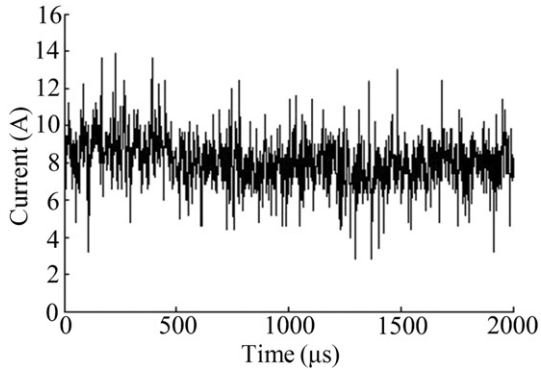

Fig. 18. Total current of longitudinal motion with locked rollers.

3.4. Cross-country experiments

Because the tracked-omni-vehicle has the same longitudinal running principle as conventional tracked vehicles, it also has comparable cross-country performance to conventional tracked vehicles. For a conventional tracked vehicle, cross-country performance is first reflected in its ability to cross obstacles. The omni-track's radius was 220 mm and the roller's radius was 19 mm; it was able to cross an approximately 260 mm height step longitudinally as shown in Fig. 19(a), which was higher than the omni-track's radius, because the rollers played the role of track grousers to climb up the step. Meanwhile, the prototype was able to cross an approximately 15 mm height step laterally as shown in Fig. 19(b), which is no higher than the roller's radius. It was demonstrated that the tracked-omni-vehicle performed well crossing obstacles in both longitudinal and lateral directions. Secondly, gradeability is important to conventional tracked vehicles in the cross-country performance. A vehicle's ultimate gradeability depends on the ground adhesion coefficient. With a large enough ground adhesion coefficient, the maximum gradeability of a conventional tracked vehicle is generally required to be no less than 60% of the slope grade. The prototype vehicle was able to climb a slope of approximately 60% longitudinally not only on firm terrain as shown in Fig. 19(c), but also on soft terrain as shown in Fig. 19(d). The maximum ground adhesion coefficient is usually no bigger than 0.8 and the ground deformation resistance is generally 0.03 [5]. Assuming that the traction of each omni-track in the longitudinal motion concentrates in its corresponding parallel direction, rather than the longitudinal direction, its ultimate slope grade will be: $0.8 \times sin(\pi/4) - 0.03 \approx 53.6\,\% < 60\,\%$. It was demonstrated again that the tracked-omni-vehicle runs with the same principle of longitudinal motion as conventional tracked vehicles.

In particular, the static stability of the tracked-omni-vehicle on a slope should also be considered because of its free rollers. In theory, its maximum stable slope grade is the same as that of a conventional tracked vehicle, except when it parks with a 45° yaw angle (the included angle between the longitudinal direction of the vehicle and the direction of slope). Considering that the ground

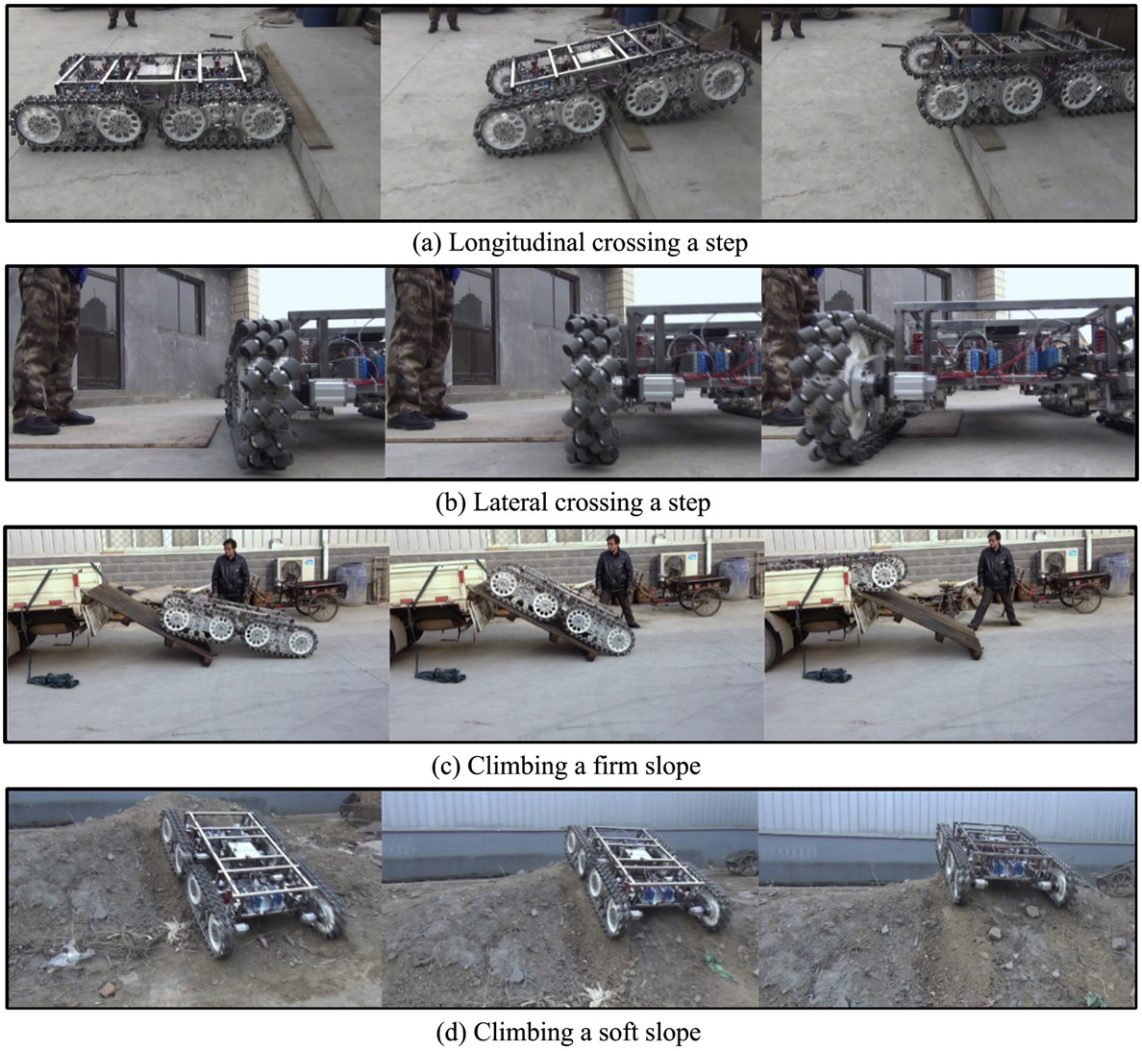

Fig. 19. Illustrations of the cross-country performance of the prototype.

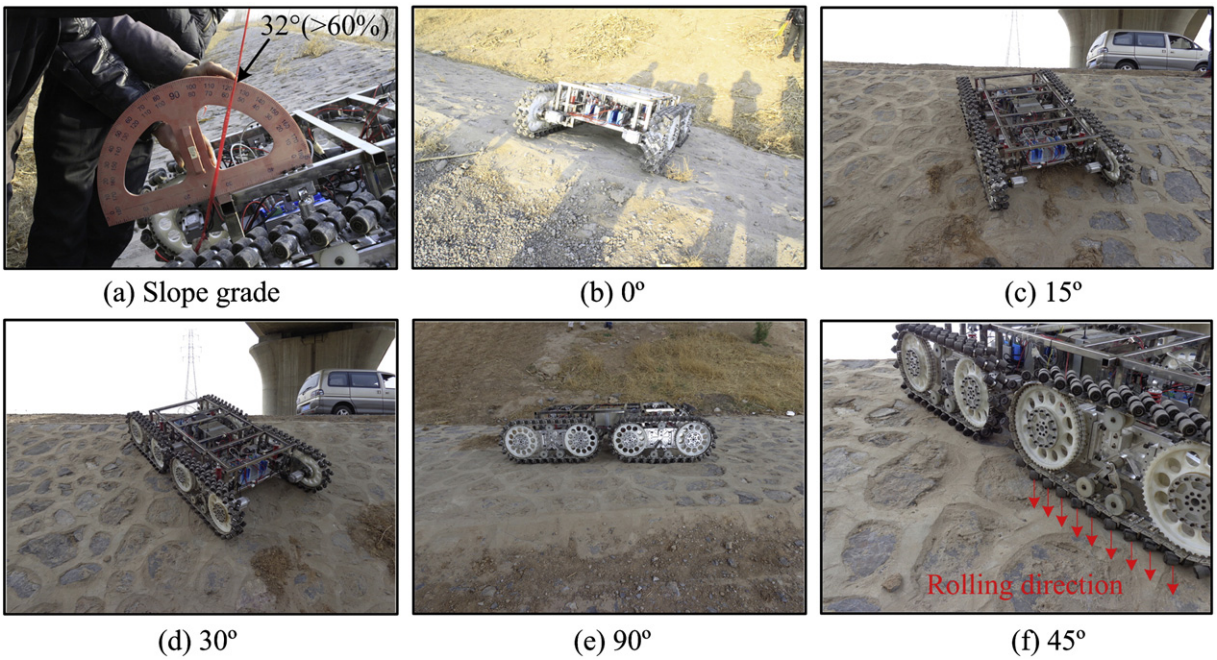

Fig. 20. Illustrations of the static stability of the prototype on a slope.

adhesion coefficient is 0.8 and when the yaw angle is 45°, its maximum stable slope grade is $0.8 \times 0.5 = 40\,\%$. The prototype was tested on a cement surface with over 60% slope grade, and it was able to keep statically stable with any yaw angle except 45° as shown in Fig. 20. Although the 45° is a singularity, the center-of-gravity position, the actual terrains and the deformations of the rollers are also related to the static stability. That is, the free rollers have almost no impact on the static stability of the tracked-omni-vehicle.

4. Conclusions

In this paper, a tracked omnidirectional and cross-country vehicle — a tracked-omni-vehicle has been invented. And its unique kinematical and dynamical theories have been analyzed. A prototype of the tracked-omni-vehicle was also presented. We have confirmed the performance of the tracked-omni-vehicle through experiments of the prototype. Hence, we can come to conclusions as follows:

1. The tracked-omni-vehicle is suitable for running on uneven terrains;
2. The tracked-omni-vehicle has superior steering motion efficiency to conventional tracked vehicles;
3. The tracked-omni-vehicle has equal longitudinal motion efficiency to conventional tracked vehicles;
4. The tracked-omni-vehicle has comparable cross-country performance to conventional tracked vehicles.

The success of the tracked-omni-vehicle has made a breakthrough in the running mode of conventional tracked vehicles and the limitations of omnidirectional vehicles in engineering applications. A new research field in design, manufacturing, and control of tracked vehicles has been opened up and omnidirectional vehicles will receive further popularization and application.

Acknowledgment

The authors would like to thank Mr. Zhiyuan Cai and the staff of Hebei Prov. Of China Run-Hui Special Mechanical Machining Corp. for their contribution.

References

[1] D. Zhao, J. Yi, Introduction to Omni-directional Wheeled Mobile Robot, Science Press, Beijing, CN, 2010.
[2] H. McGowen, Navy omni-directional vehicle (ODV) development: where the rubber meets the deck, Nav. Eng. J. 112 (4) (2000) 217–228, http://dx.doi.org/10.1111/j.1559-3584.2000.tb03332.x.
[3] Airtrax, Omni-directional Technology: Changing the Way Vehicles Move, http://www.airtrax.com/.
[4] J.W. Kang, H.S. Hong, B.S. Kim, M.J. Chung, Assistive mobile robot systems helping the disable walkers in a factory environment, Int. J. ARM 9 (2) (2008) 42–52.
[5] M. Wang, Y. Zhao, J. Zhu, Driving Principle of Tank, National Defense Industry Press, Beijing, CN, 1983.
[6] W. Merhof, E. Hackbarth, Running Mechanics of Tracked Vehicle, National Defense Industry Press, Beijing, CN, 1989.
[7] F. Sun, C. Zhang, Technologies for the Hybrid Electric Drive System of Armored Vehicle, National Defense Industry Press, Beijing, CN, 2008.

[8] M. West, H. Asada, Design of a holonomic omnidirectional vehicle, Proceedings the 1992 IEEE International Conference on Robotics and Automation, IEEE, Nice, France, 1992, pp. 97–103, http://dx.doi.org/10.1115/1.2826230.
[9] R. Damoto, W. Cheng, S. Hirose, Holonomic omni-directional vehicle with new omni-wheel mechanism, Proceedings of the 2001 IEEE International Conference on Robotics and Automation, IEEE, Seoul, Korea, 2001, pp. 773–778, http://dx.doi.org/10.1109/ROBOT.2001.932644.
[10] P. Chen, S. Mitsutake, T. Isoda, T. Shi, Omni-directional robot and adaptive control method for off-road running, IEEE Trans. Robot. Autom. 18 (2) (2002) 251–256, http://dx.doi.org/10.1109/TRA.2002.999654.
[11] P. Chen, S. Koyama, S. Mitsutake, T. Isoda, Automatic running planning for omni-directional robot using genetic programming, Proceedings of the 2002 IEEE International Symposium on Intelligent Control, IEEE, Vancouver, Canada, 2002, pp. 485–489, http://dx.doi.org/10.1109/SIC.2002.1157811.
[12] K. Tadakuma, R. Tadakuma, H. Kinoshita, K. Nagatani, K. Yoshida, M. Udengaard, K. Iagnemma, Mechanical design of cylindrical track for sideways motion, Proceedings of 2008 IEEE International Conference on Mechatronics and Automation, IEEE, 2008, pp. 161–167, http://dx.doi.org/10.1109/ICMA.2008.4798744.
[13] K. Tadakuma, R. Tadakuma, K. Nagatani, K. Yoshida, S. Peters, M. Udengaard, K. Iagnemma, Crawler vehicle with circular cross-section unit to realize sideways motion, Proceedings IEEE/RSJ International Conference on Intelligent Robots and System, IEEE, 2008, pp. 2422–2428, http://dx.doi.org/10.1109/IROS.2008.4651223.
[14] S. Hirose, S. Amano, The VUTON: high payload, high efficiency holonomic omni-directional vehicle, Proceedings of 6th International Symposium on Robotics Research, IFRR, 1993, pp. 253–260.
[15] Y. Xiong, Fundamentals of Robot Technology, Huazhong University of Science and Technology Press, Wuhan, CN, 1996.
[16] Y. Wang, D. Chang, Motion performance analysis and layout selection for motion system with four Mecanum wheels, Chin. J. Mech. Eng. 45 (5) (2009) 307–310.
[17] O. Diegel, A. Badve, G. Bright, J. Potgieter, S. Tale, Improved Mecanum wheel design for omni-directional robots, Proceedings of the 2002 Australasian Conference on Robotics and Automation, AARA, 2002, pp. 117–121.
[18] C. Leng, Q. Cao, Anisotropy of 4-wheeled omnidirectionally mobile robots, CAAI Trans. Intell. Syst. 2 (3) (2007) 45–51.